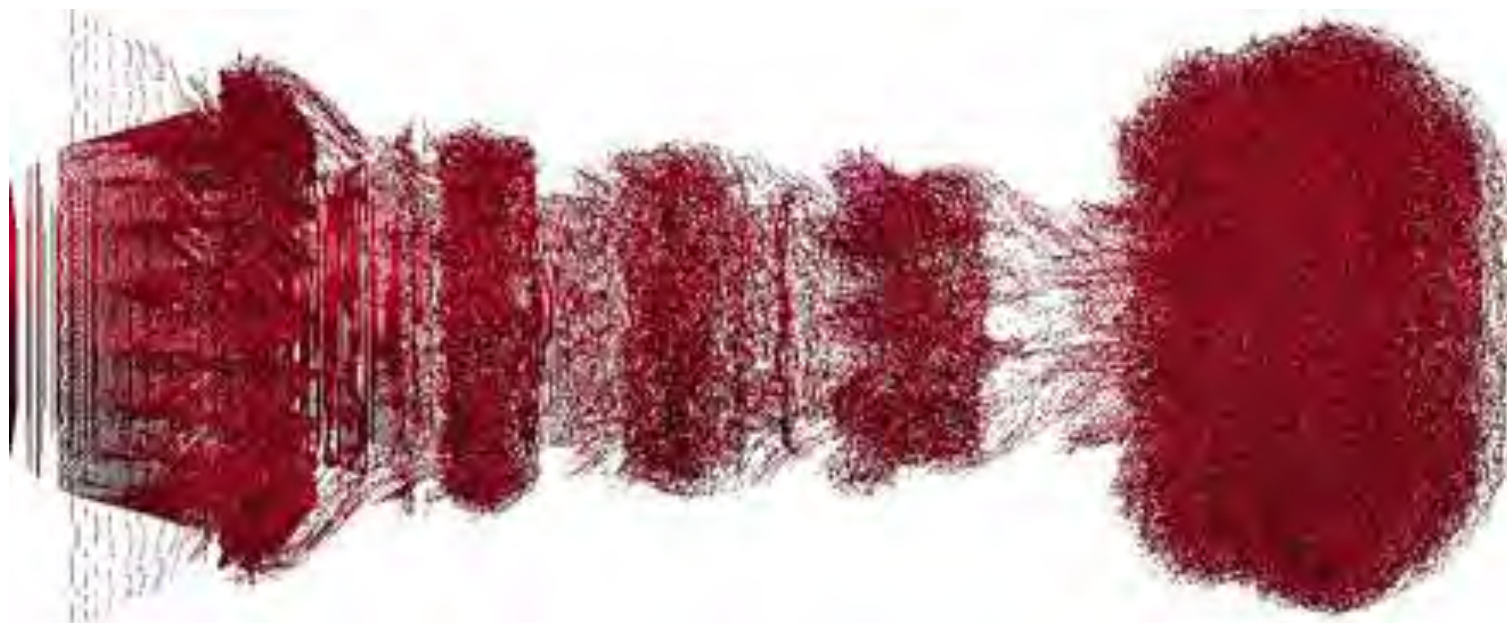


# Vortex Method Applications

Peter S. Bernard  
University of Maryland



## **Vortex Methods**

**Flow field is represented using gridfree vortex elements**

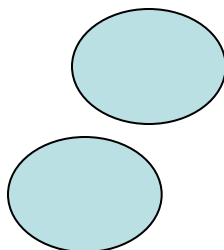
**Navier-Stokes equation governs the dynamics of the freely convecting vortex elements**

**Velocity is recovered from the vortices using the Biot-Savart law**

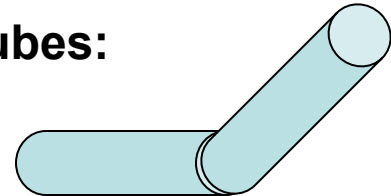
**For turbulent flow simulation vortex methods operate as a LES:  
not economical to resolve the smallest scales.**

# Vortex Elements

“Blobs”



or: filaments made up of tubes:



	Viscous Diffusion	Vortex Stretching
Blob methods	Accurate, if: blobs overlap occasional remeshing	Unstable - depends on calculation of velocity derivatives.
Filament methods	Not straightforward.	Convect tube end points.

## Filament methods:

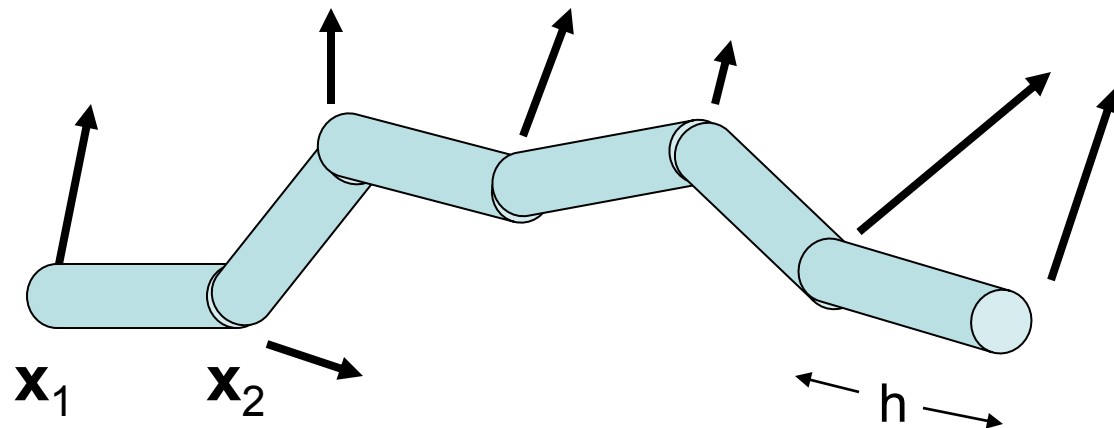
- preferred for turbulent flow simulation since vortex stretching is an essential and dominant flow process.
- viscous diffusion is not significant away from walls.
- viscous dissipation is "subgrid" and can be modeled via loop removal.

## Blob methods:

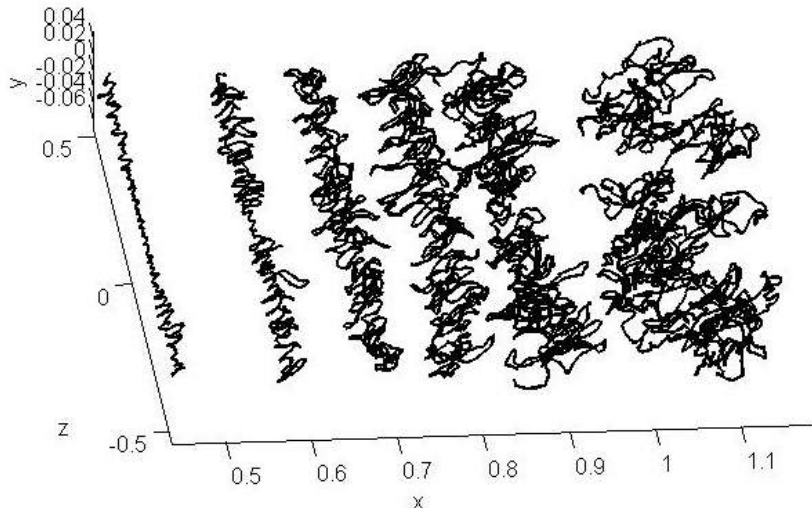
- rarely applied to turbulence due to vortex stretching instability
- best suited to moderate Reynolds number flows where viscous diffusion is an essential aspect of the dynamics (e.g. laminar vortex rings, low speed jets).

# Vortex Filament Scheme

- Computational elements: straight vortex tubes linked end-to-end forming filaments.
- Convect tubes via their endpoints: this models the convection and vortex stretching term in the equations of motion.
- Circulation  $\Gamma$  on filaments is constant (Kelvin's Theorem)
- Tubes subdivide when stretched beyond length  $h$ .



**In turbulent flow:  
vortex filaments stretch  
and fold - taking energy to  
small, dissipative scales**

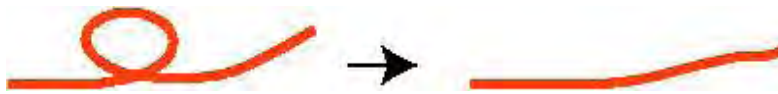


**Not economical to resolve the dissipation scales.**

**Moreover, viscous diffusion would have to be modeled directly.**

**Loop removal offers a means around the impasse.**

**loop removal** can be used as a "sub-grid model" (Chorin).



**Vortex loops are removed as they form, thus providing spatially intermittent local dissipation: in fact, vortex loops contribute only to the local velocity field.**

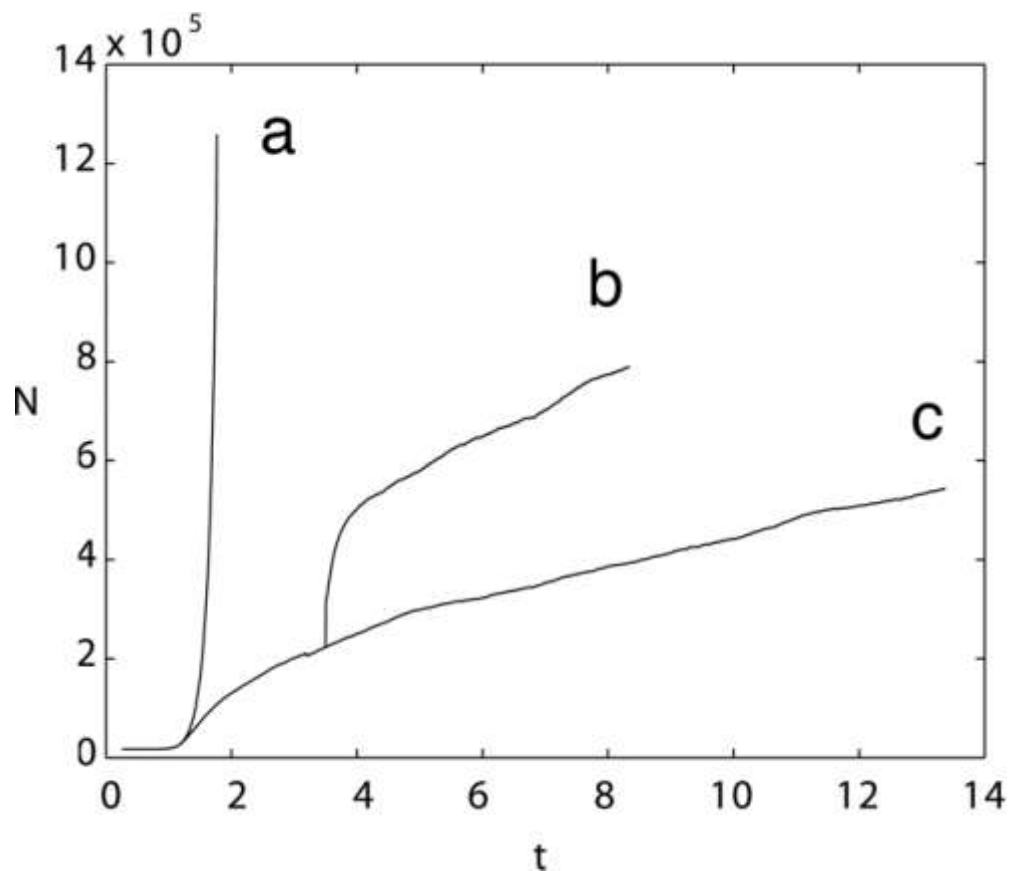
**In principle, energy is removed at inertial range scales without the hardship of computing energy transfer to the smallest scales.**

**Loop removal is non-diffusive (unlike traditional sub-grid models).**

**Does not prevent or interfere with backscatter: (e.g. filaments combine to form larger scale structures).**

**Prevents runaway growth in the number of tubes.**

## Number of tubes vs. time



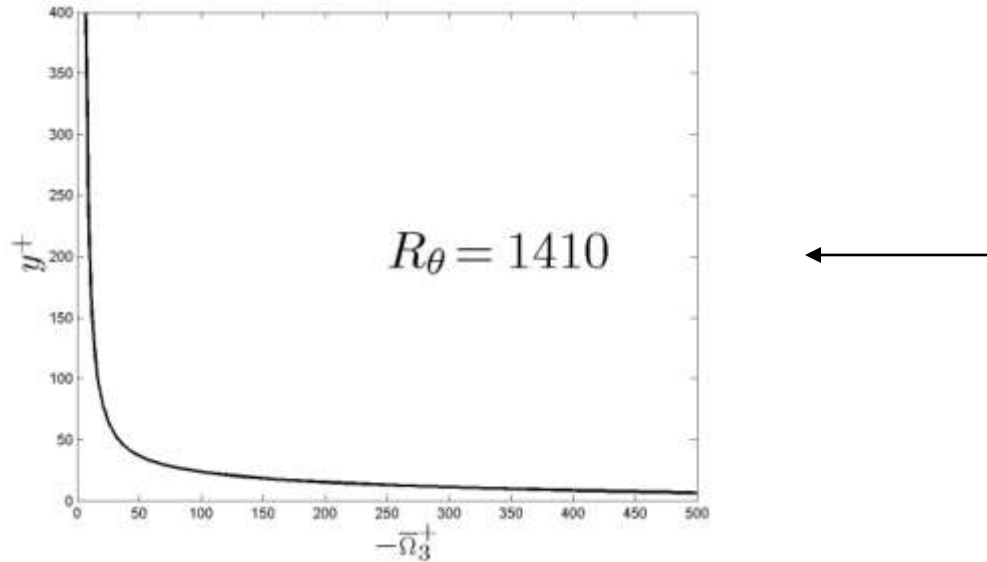
**a:** without loop removal,  
 $h = 0.0375$  (max  
tube length)

**b:** with loop removal,  
 $h = 0.025$

**c:** with loop removal  
 $h = 0.0375$

# Near-Wall Considerations

Flow near solid walls contains strong vorticity gradients that determine viscous production of new vorticity.



Mean vorticity near wall in a turbulent boundary layer

In general, LES is not appropriate next to walls since all scales need to be resolved.

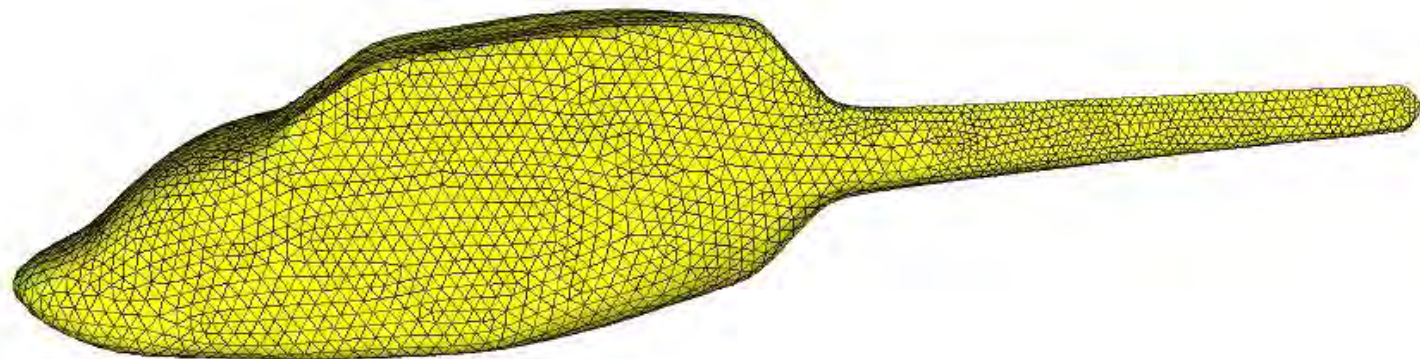
DNS resolution is necessary.

**Near-wall vorticity gradients are not readily accounted for via gridfree vortex elements.**

**All viscous effects must be computed next to a wall.**

**Solid surfaces are often specified via triangulations.**

**Sheet-like vortices on a thin prismatic wall mesh can be used to efficiently resolve the steep vorticity gradients.**

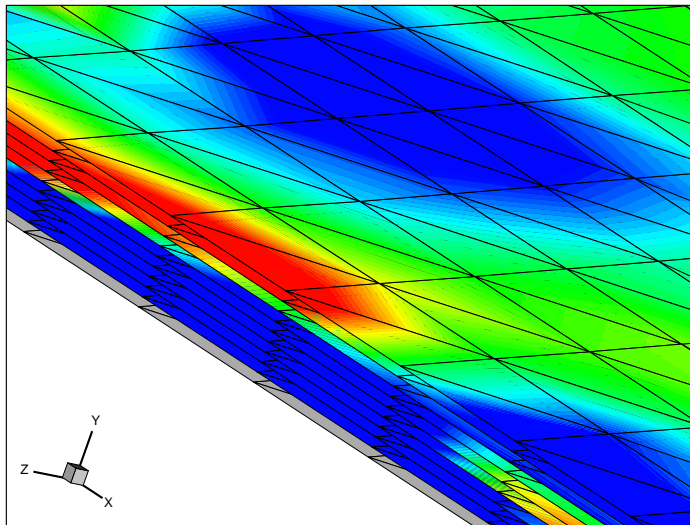


**With these constraints in mind:**

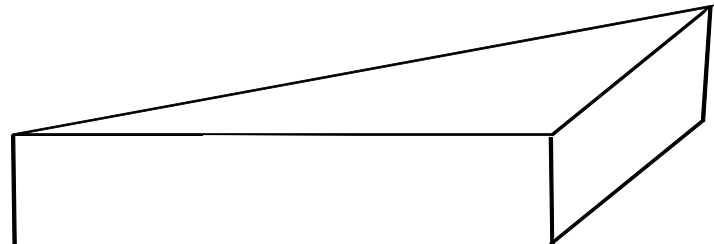
**a fine resolution finite volume scheme is employed to solve the full 3D, viscous vorticity equation on a thin region ( $y^+ < 30-50$ ) next to boundaries.**

**Triangular prism mesh (usually 11 layers) is grown from surface triangles.**

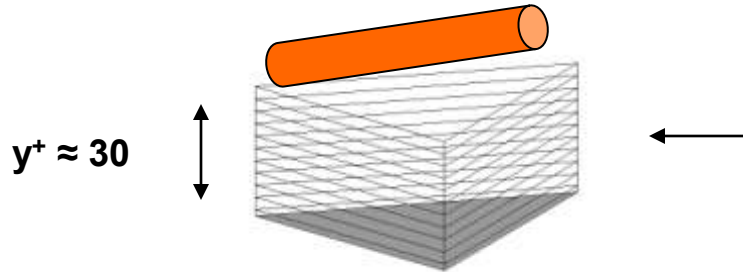
**No-slip BC at wall; constant flux BC at top sheet layer.**



$$\Delta y^+ \approx 3$$



$$\Delta z^+ \approx 30$$



**New filaments are produced from the vorticity arriving at the top layer.**

**Orientation of new vortices is determined from local vorticity.**

**The circulation strength  $\Gamma$  is determined by the condition that the prism and new tube have the identical far field velocity:**

$$\Gamma|s| = |\Omega|V_T$$

**$V_T$  = prism volume       $s$  = axial vector on tube.**

## Velocity Computation

$$\mathbf{U}_{\text{total}} = \mathbf{U}_{\text{tubes}} + \mathbf{U}_{\text{sheets}} + \mathbf{U}_{\text{potential}}$$

**For N tubes:**  $\mathbf{U}_{\text{tubes}} = -\frac{1}{4\pi} \sum_{i=1}^N \frac{\mathbf{r}_i \times \mathbf{s}_i}{|\mathbf{r}_i|^3} \Gamma_i \phi(|\mathbf{r}_i|/\sigma),$

**where**  $\mathbf{x}_i = (\mathbf{x}_{1,i} + \mathbf{x}_{2,i})/2$ ,  $\mathbf{r}_i = \mathbf{x} - \mathbf{x}_i$ ,  $r_i = |\mathbf{r}_i|$ ,  $\mathbf{s}_i = \mathbf{x}_{2,i} - \mathbf{x}_{1,i}$

$$\phi(|\mathbf{r}_i|/\sigma) = 1 - \left(1 - \frac{3}{2}(|\mathbf{r}_i|/\sigma)^3\right) e^{-(|\mathbf{r}_i|/\sigma)^3},$$

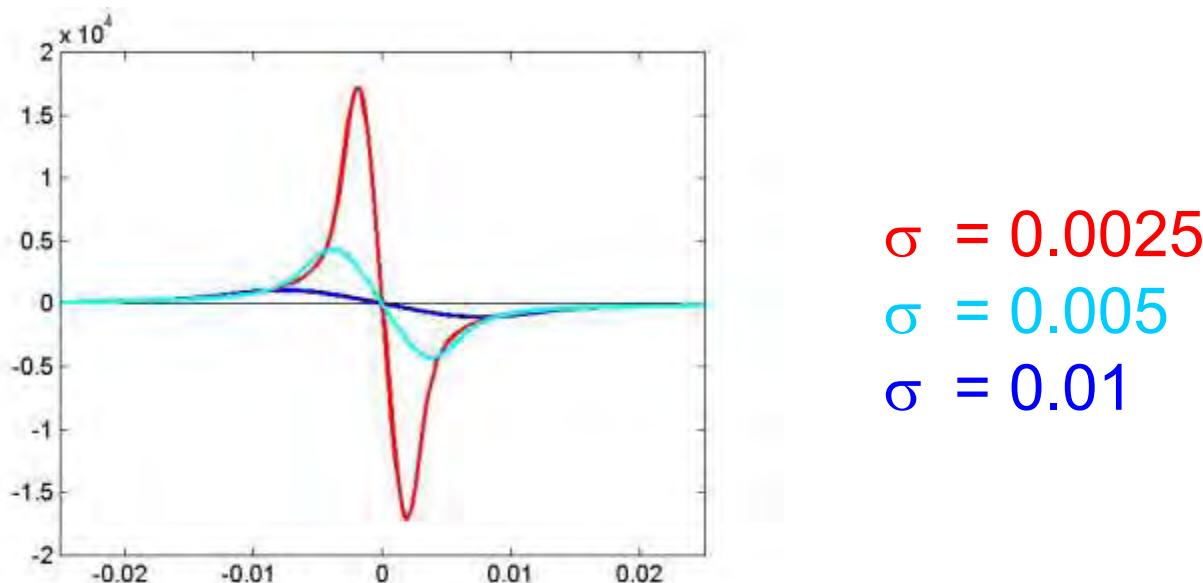
desingularizes the Biot-Savart kernel.

$\mathbf{U}_{\text{sheets}} \rightarrow$  sum over individual contributions: near field from exact formulas, far field as equivalent tubes.

$\mathbf{U}_{\text{potential}} \rightarrow$  sum over surface sources to enforce non-penetration.

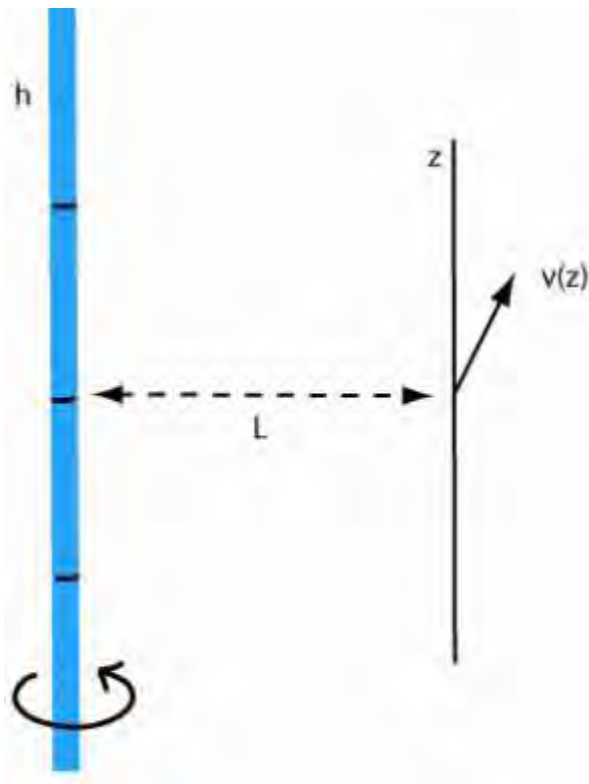
**Variations of the velocity over distances smaller than the tube length cannot be known accurately.**

**For example,  $\sigma$  has some effect on the local velocity surrounding any vortex - but it is not physical.**

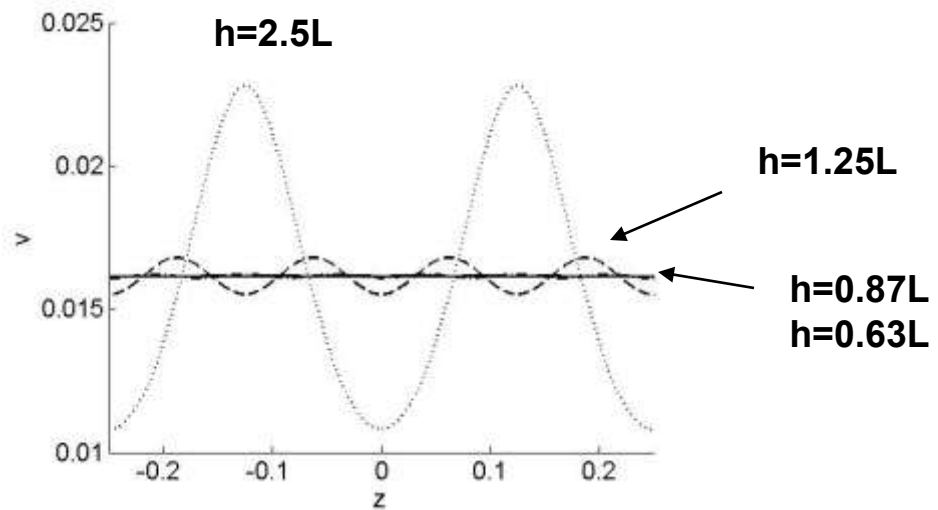


**Velocity on a line through a vortex.**

## Approximation to Biot-Savart law for a tube introduces local errors:



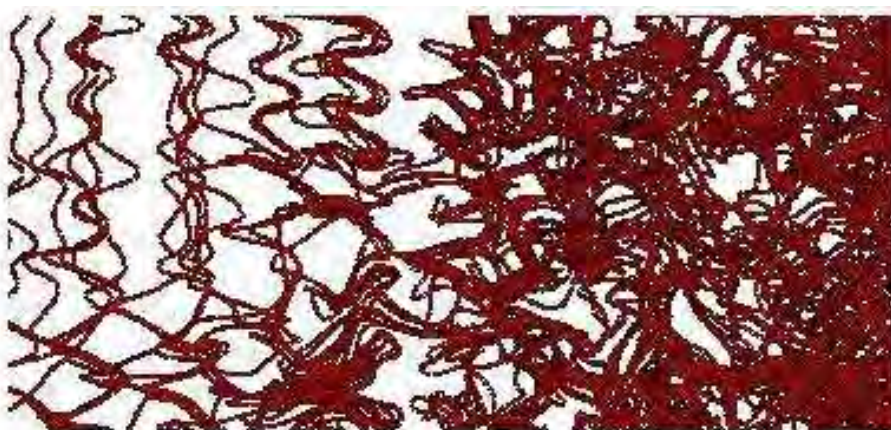
In this example,  $v(z)$  should be a constant, independent of  $z$ , and it is once the tube size  $h < L$ .



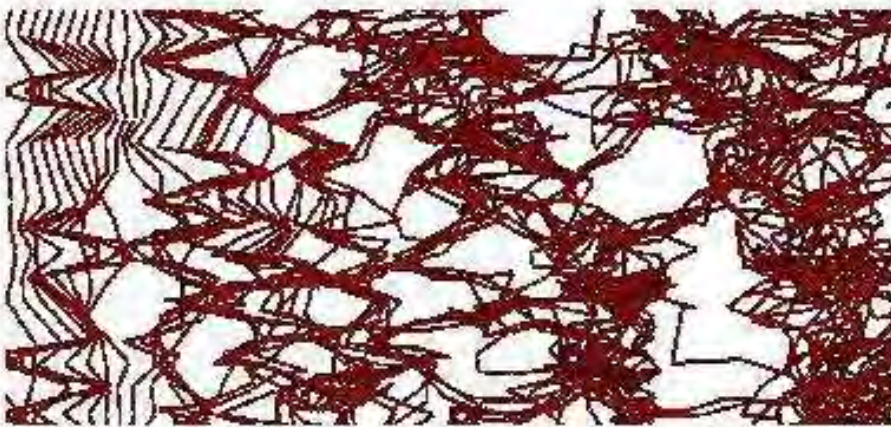
$h$ ,  $\Gamma$  and  $\Delta t$  should be kept as small as is practical

**Magnitude of  $h$  has a significant visual effect on simulations:**

**$h = 0.005$**

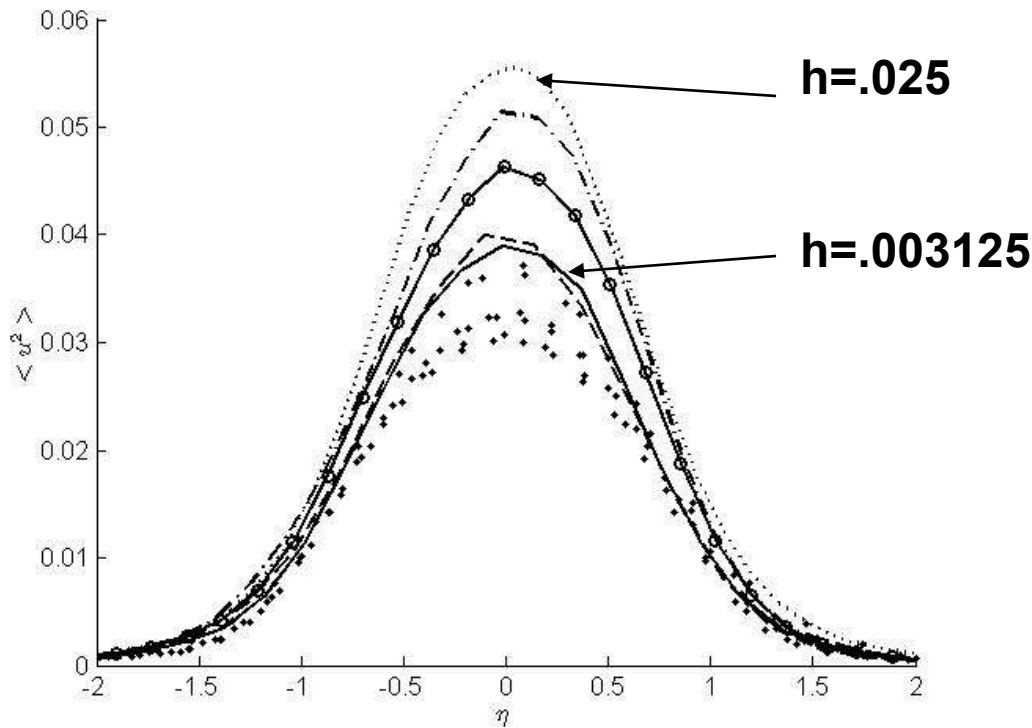


**$h = 0.025$**



**Large  $h$  is linked to over-prediction of Reynolds Stresses in some cases.**

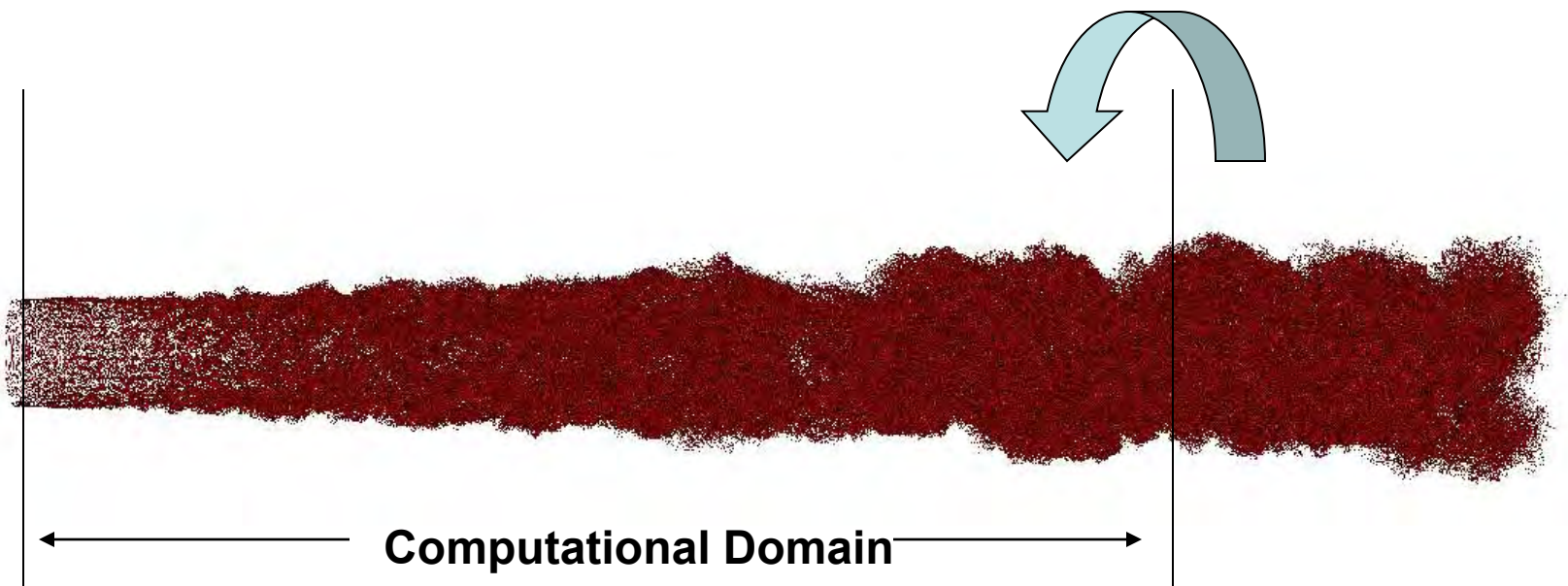
**In the case of a plane mixing layer:**



**Predictions converge to experimental values as  $h$  is reduced:  
0.025 → 0.003125**

- Bell/Mehta experiment

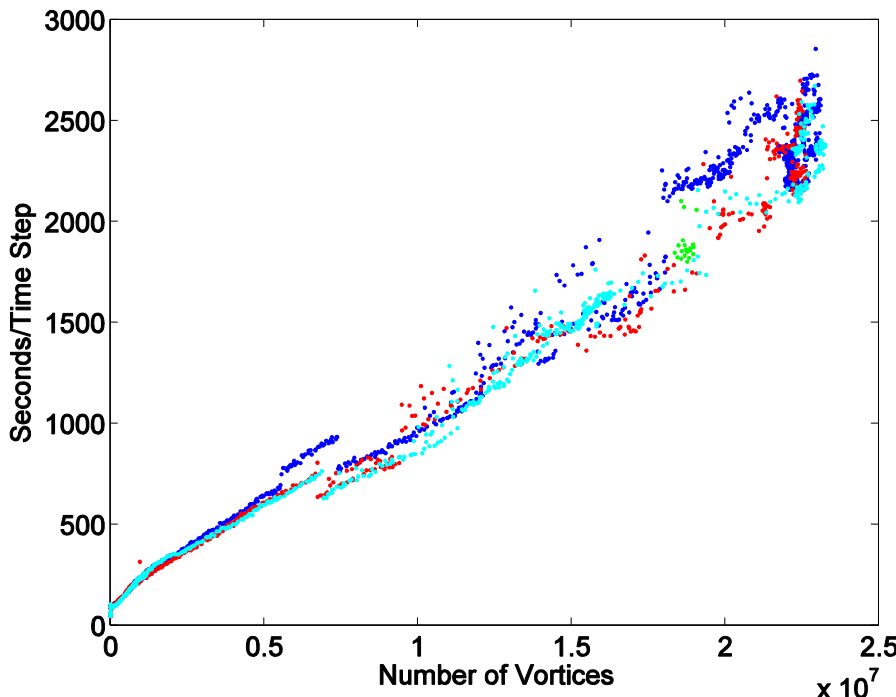
**Use of Biot-Savart law means that in many applications vorticity outside the domain of interest may contribute to the velocity field.**



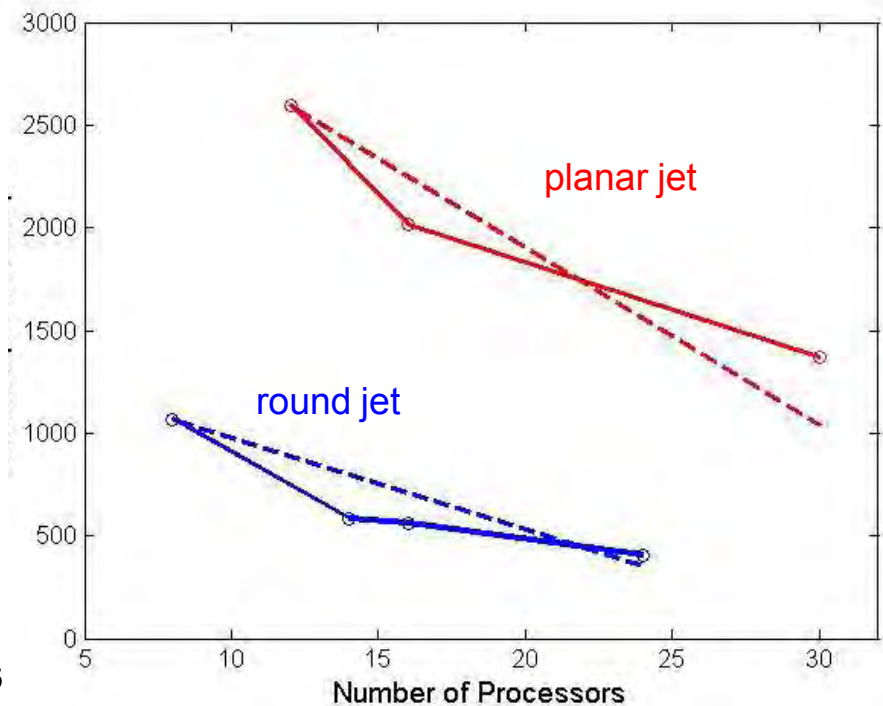
# Numerical Aspects of Velocity Computation

$O(N^2)$  cost reduced to  $O(N)$  via use of an adaptive Fast Multipole Method (Greengard & Rohklin).

Parallel efficiency is excellent through 22 processors.



**$O(N)$  scaling in the FMM**



Parallel efficiency. (Dashed – ideal).  
- 13M tubes  
- 10M tubes + 8 periodic extensions

## **Summary of Numerical Parameters (Filament Calculations)**

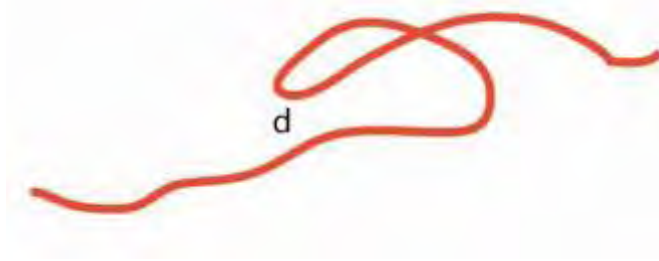
**h – tube length**

**$\Delta t$  - time step**

**$\Gamma$  - circulation**

**$\sigma$  - smoothing parameter in Biot-Savart Law**

**d - criterion for loop removal**



Among the advantages of vortex methods:

The representation of vortices in terms of their end points and circulation represents a gain in efficiency over grid-based methods.

Vortices remain sharp (without dissipation) as they convect.

Opportunity to employ non-diffusive "subgrid" modeling.

Gridding requirements are easier to accommodate than grid-based schemes (e.g. number of prisms  $\sim \text{Re}^{3/2}$ ).

Direct view of vortical structures provides a new way of exploring the physics of turbulence.

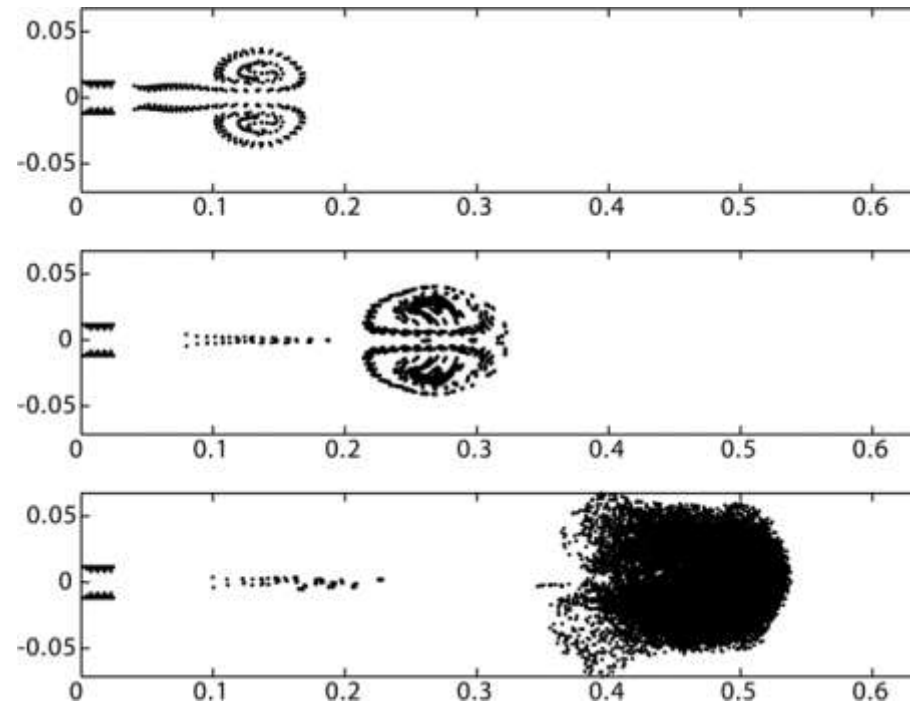
# Some Applications of the Vortex Filament Scheme

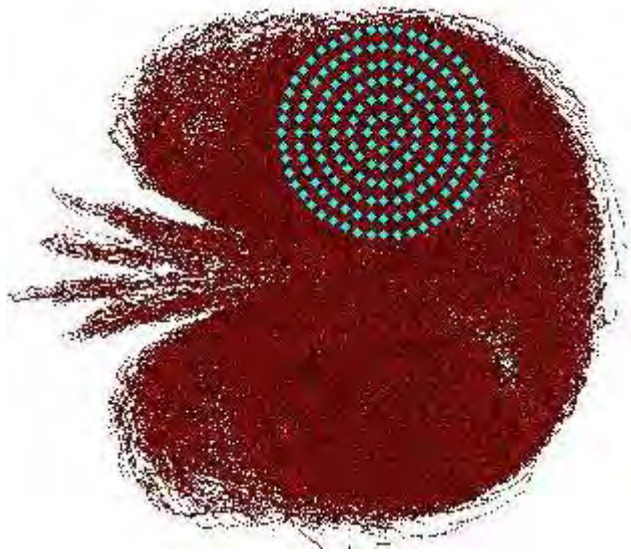
1. "Isotropic Turbulence"
2. Spatially developing shear layer
3. Boundary layer
4. Automotive Flows
5. Rotorcraft Flows
6. Co-flowing round jet

"Isotropic" Turbulence

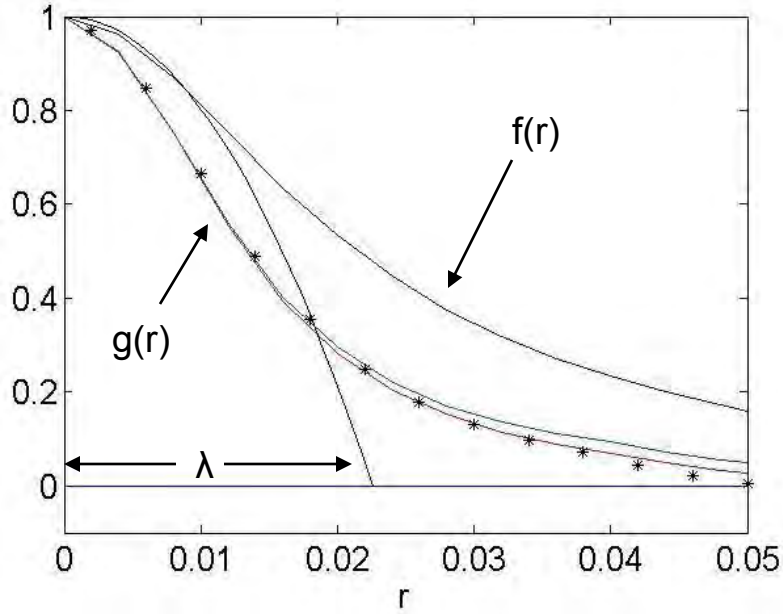
A more or less isotropic region of turbulence is created from a short duration pulse of a planar jet.

- Orifice has unit width.
- 20 layers of filaments,  $h=0.005$ .
- Incoming circulation corresponds to Poiseulle Flow at the orifice exit.
- 4 periodic extensions to either side used in computing velocities.





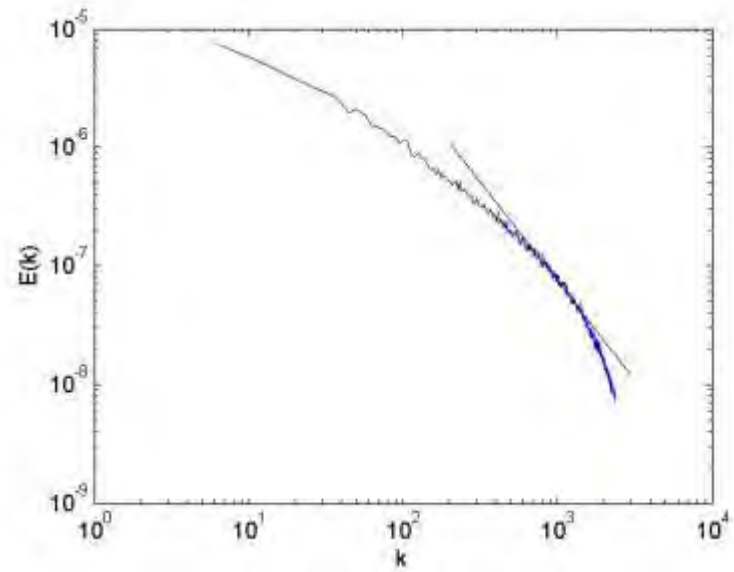
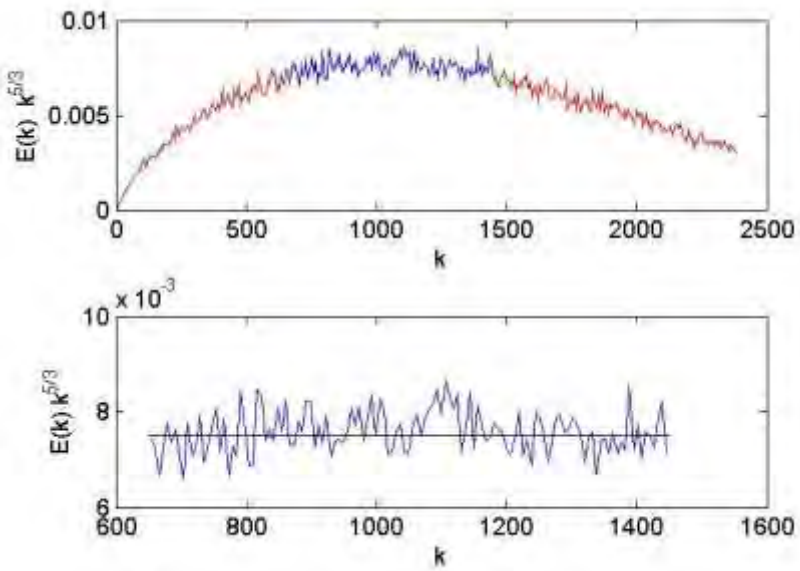
**Turbulence statistics  
computed from spanwise  
velocity traces.**



**Two point longitudinal,  $f(r)$ , and transverse,  $g(r)$ , correlation functions**

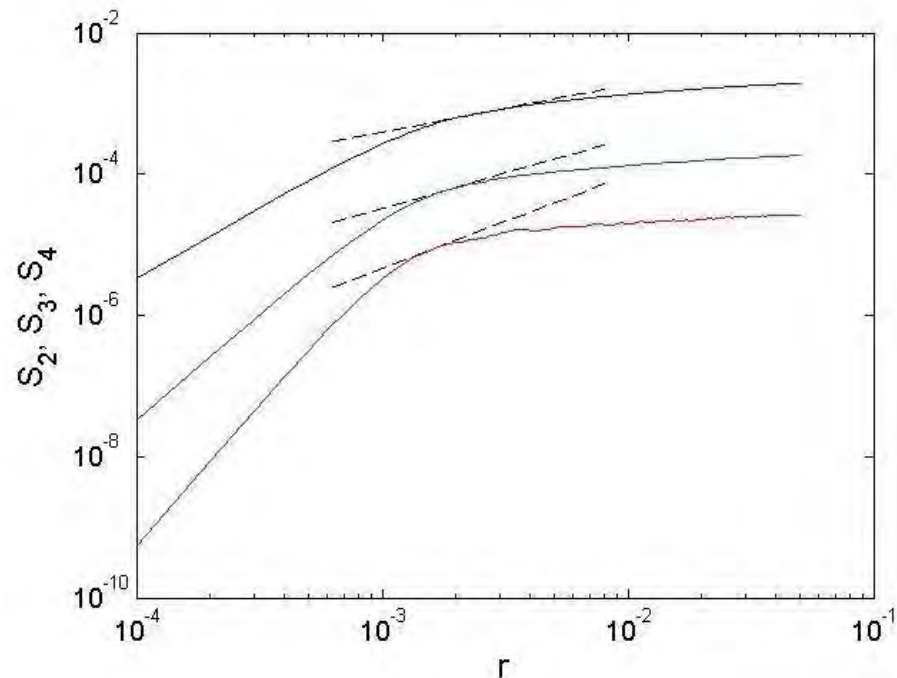
**Symbols show consistency with the isotropy condition:**

$$g(r) = f(r) + r/2 \frac{df}{dr}(r)$$



1D spectra and Kolmogorov law.

Assuming that the universal form:  $E(k)=0.53 \varepsilon^{2/3} k^{-5/3}$  holds,  
the dissipation  $\varepsilon$  can be computed.



Structure functions  $S_2(r)$ ,  $S_3(r)$ ,  $S_4(r)$  where  $S_n(r) = \overline{|u(x+r)-u(x)|^n}$ .

Dashed lines have slopes,  $2/3$ ,  $1$ ,  $4/3$ , respectively.

$\varepsilon$  can also be computed from the universal form  $S_n(r) = 2.13 \varepsilon^{2/3} r^{2/3}$

## Reynolds Number

Substituting  $\varepsilon$  and  $\lambda$  into the isotropic identity  $\varepsilon = 15 \nu u'^2 / \lambda^2$  yields

$$R_e = UL/\nu = 15 u'^2 / (\lambda^2 \varepsilon)$$

and then

$$R_\lambda = u' \lambda / \nu = R_e u' \lambda.$$

Furthermore, Kolmogorov length and time scales may be computed (non-dimensionalized with  $U,L$ ):

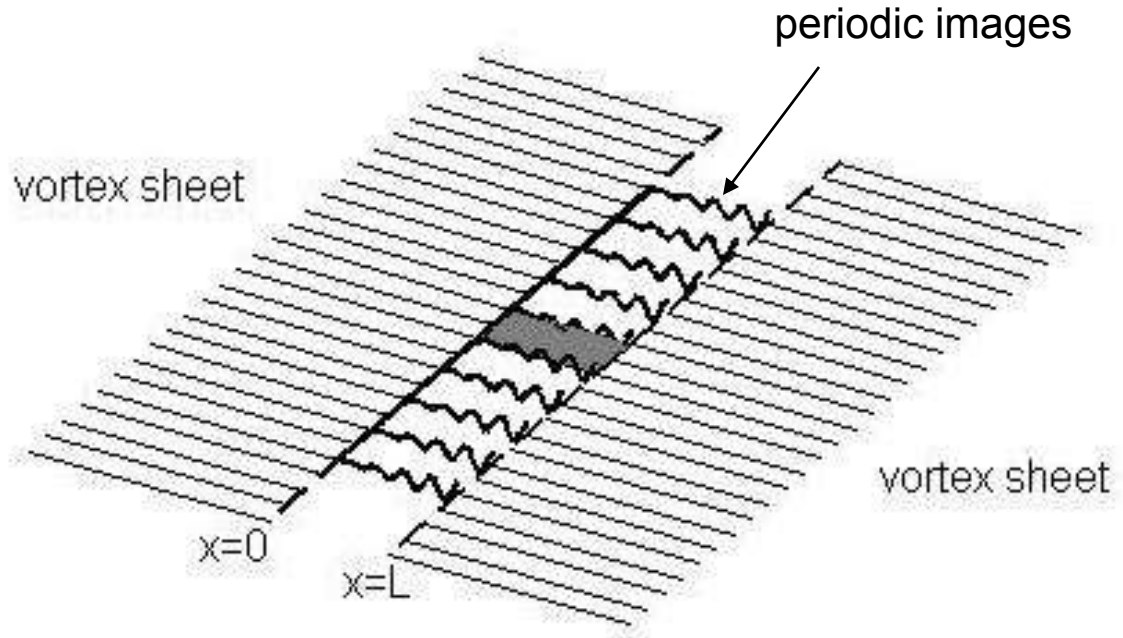
$$\eta = R_e^{-3/4} \varepsilon^{-1/4} \quad t_d = (R_e \varepsilon)^{-1/2}$$

For blob flow with  $\zeta = 0.01$ :

$$R_\lambda = 71 \quad R_e = 155354 \quad \lambda = 0.023 \quad \eta = 0.0017 \quad \varepsilon = 0.00008 \quad t_d = 0.23$$

# Mixing Layer

# Mixing Layer



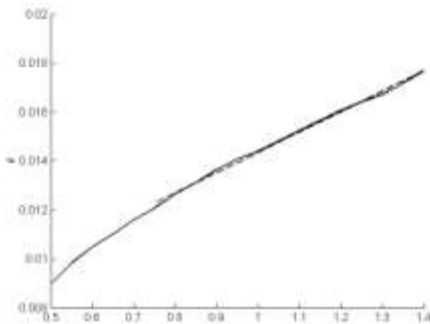
**Spatial extent of one periodic image of the shear layer:**

**2000  $\theta$  X 1000  $\theta$  in the x and z directions, respectively,**

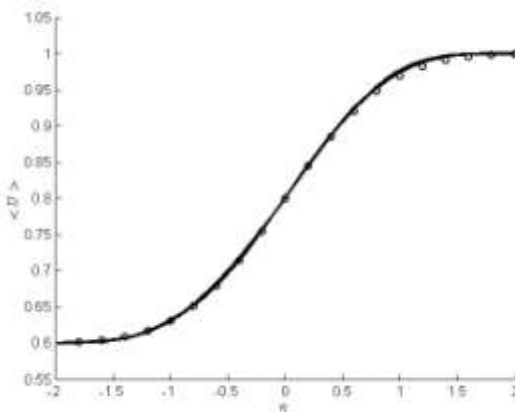
**where  $\theta$  is the momentum thickness:**

$$\theta \equiv \int (U_h - \bar{U})(\bar{U} - U_l) dy / (U_h - U_l)^2$$

**Quantitative predictions are consistent with Bell/Mehta experiment:**

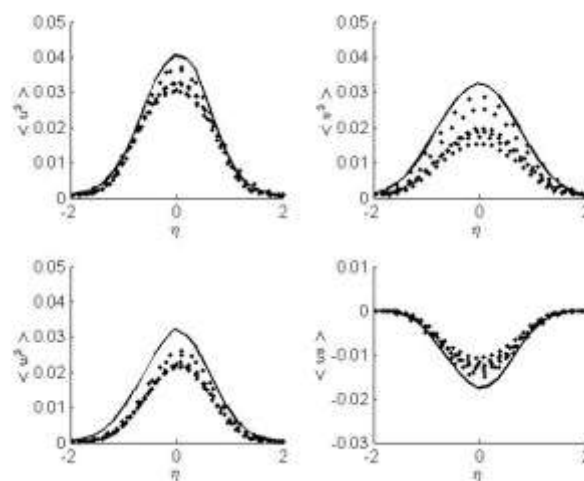


**Correct linear growth in momentum thickness.**



**Mean velocity is self-similar and matches error function.**

**Reynolds stresses close to experiment.**



**Experimental observations have categorized 3 kinds of vortex structure in transition:**

**1. Roller/Rib**

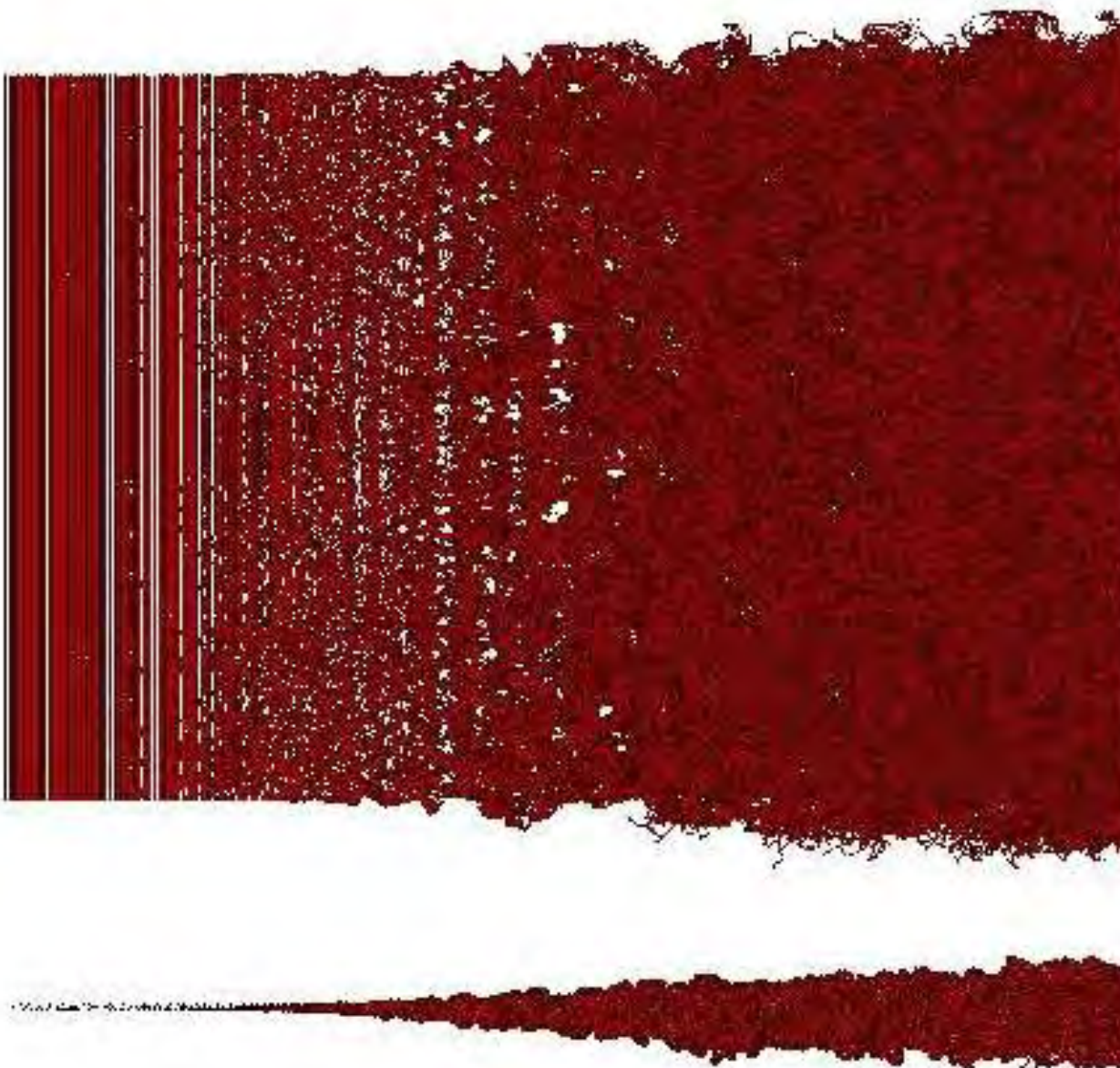
**2. Vortex lattice (chain link fence)**

**•Response to asymmetric forcing.**

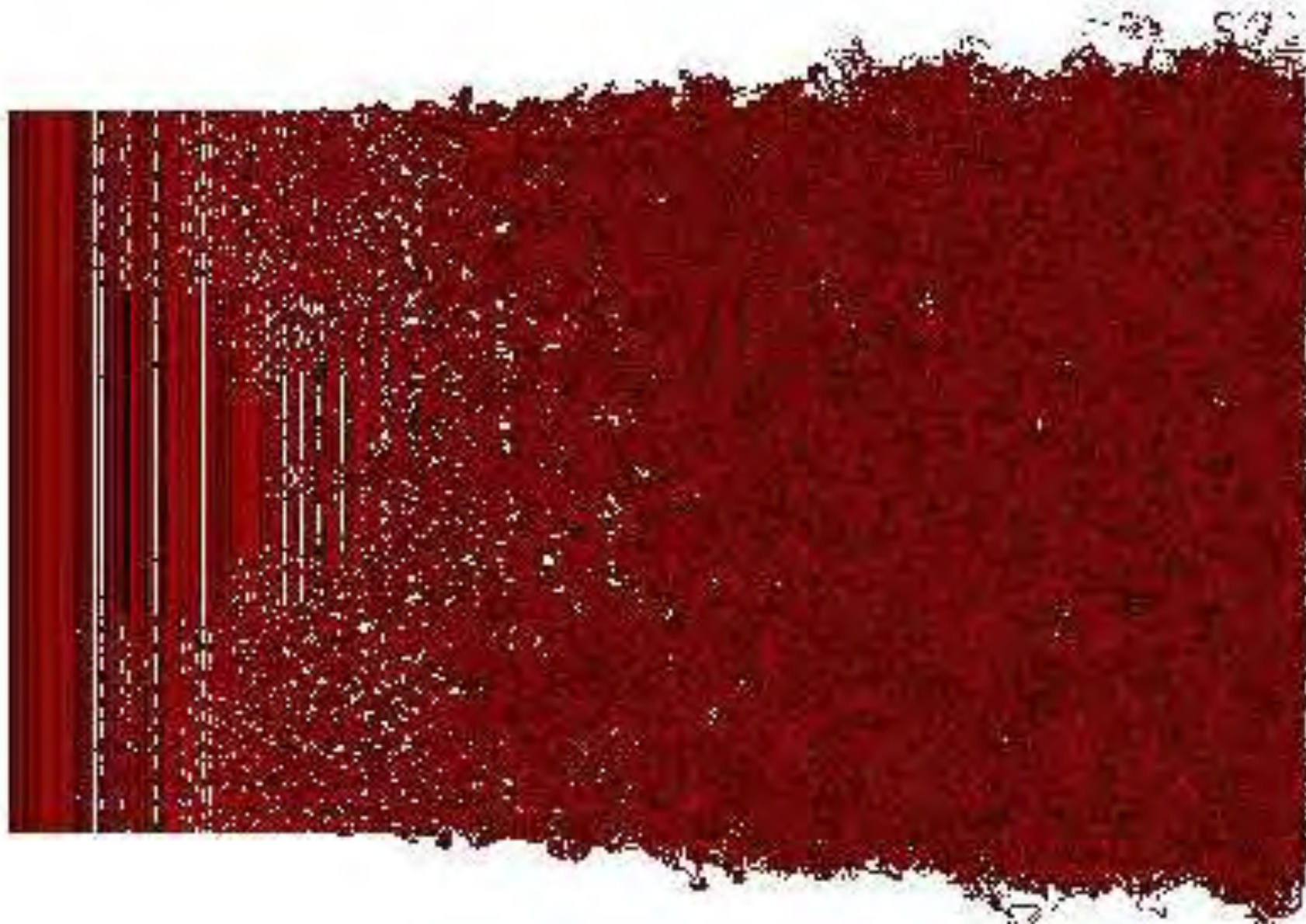
**3. Oblique roller vortices with partial pairing.**

**•Associated with upstream turbulence.**

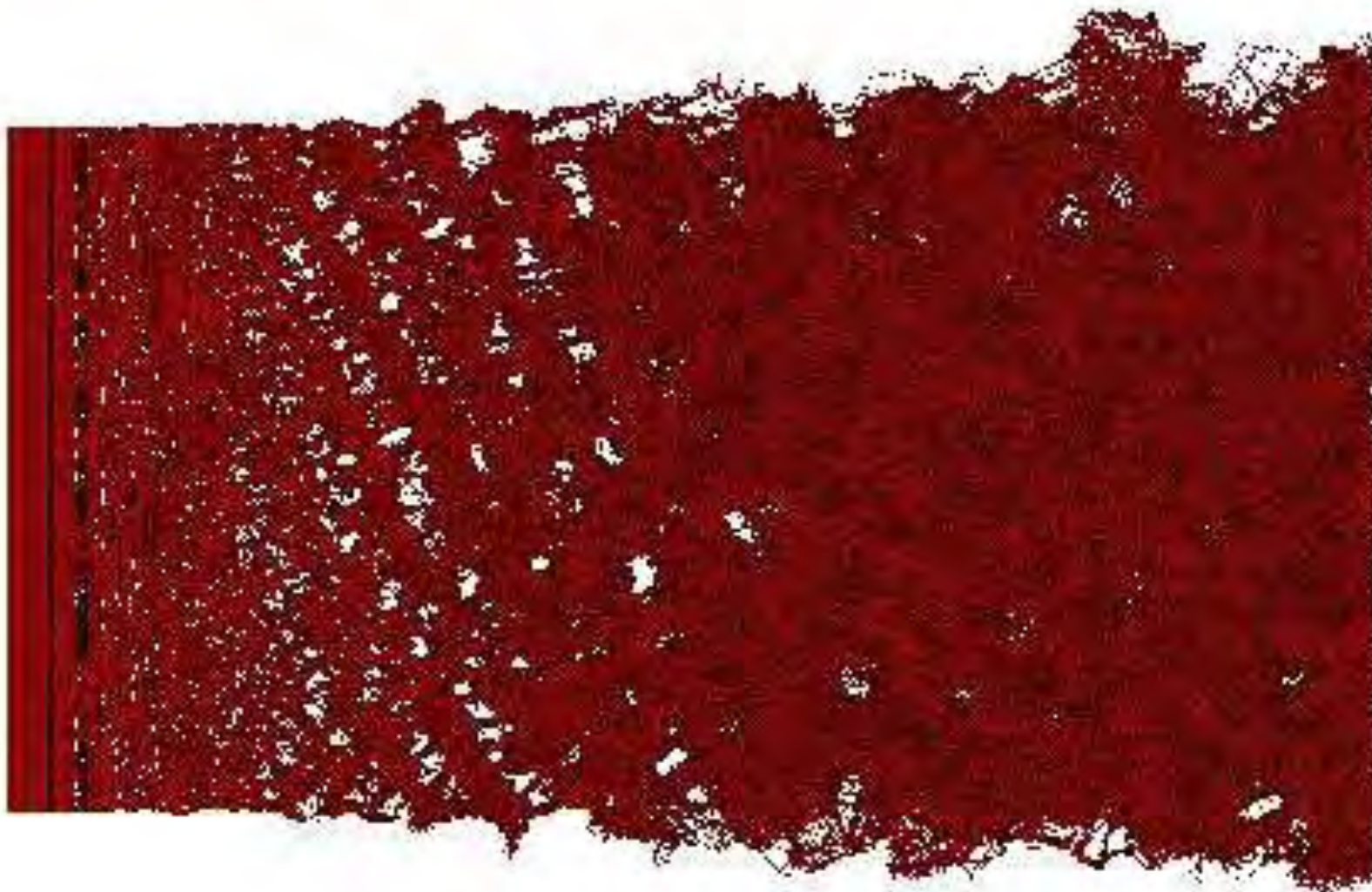
## Roller/rib transition



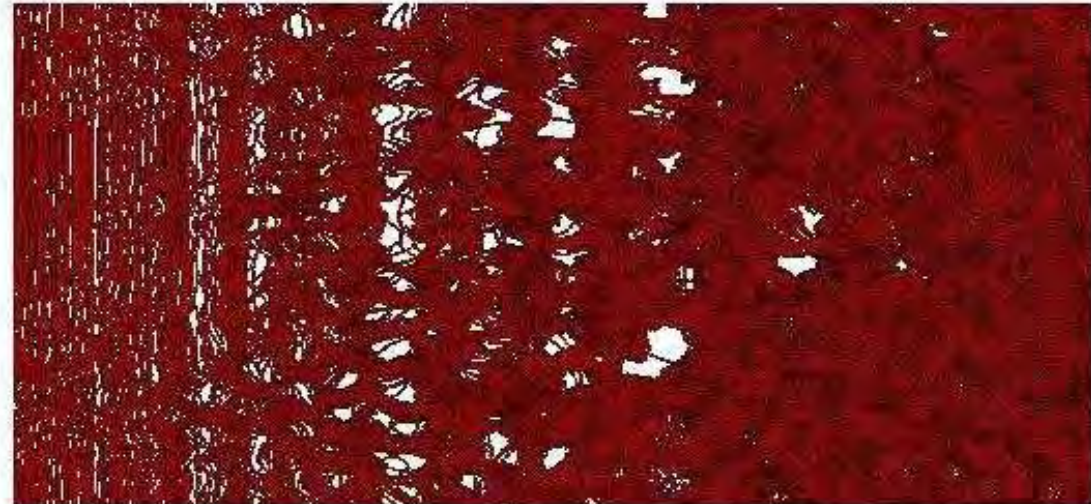
## Vortex lattice/chain link fence transition



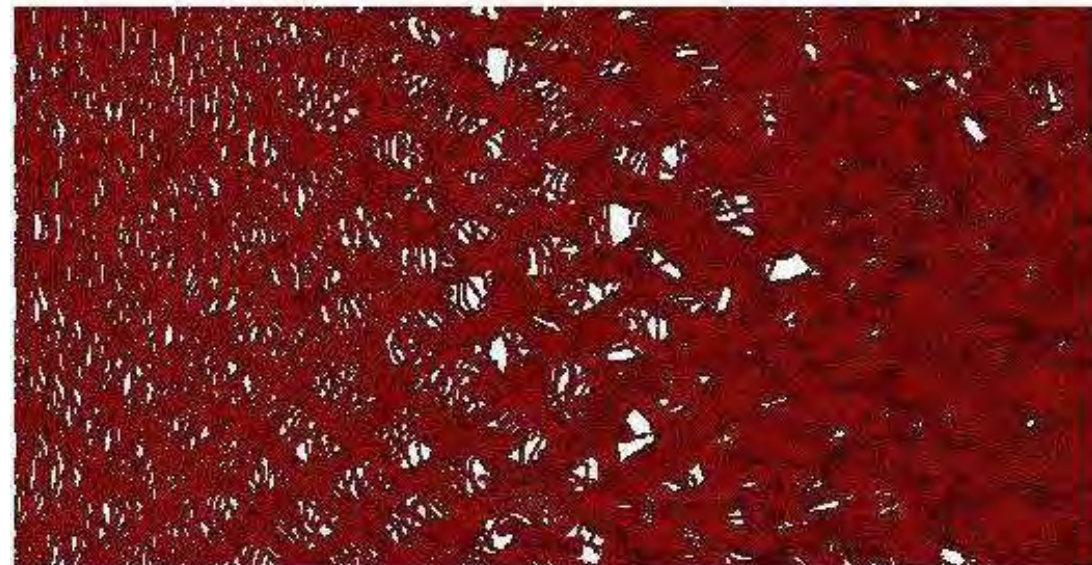
## Oblique roller vortices with partial pairing



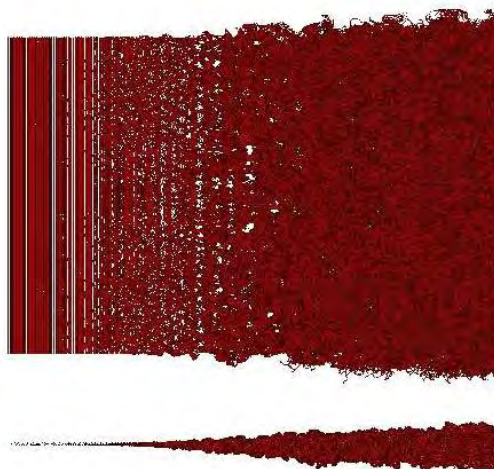
**Close up view  
of roller/ribs**



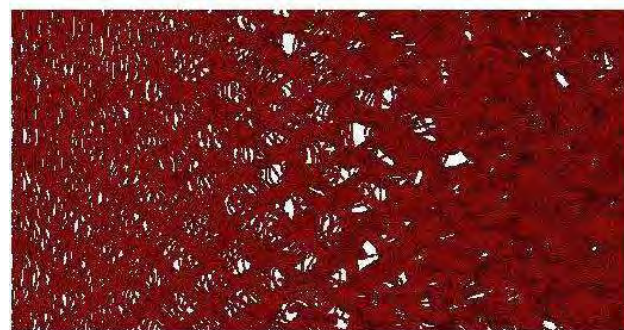
**Close up view  
of lattice**



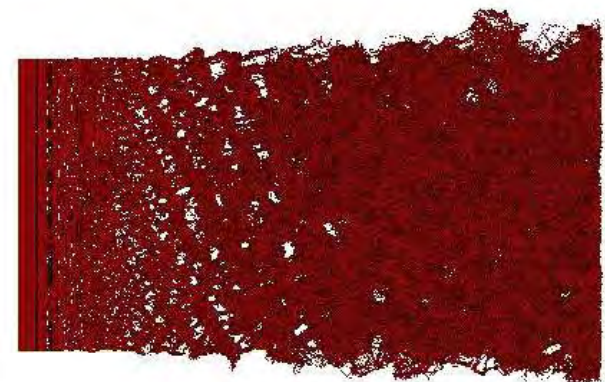
## Three transition modes seen in experiment:



**Roller/Rib**



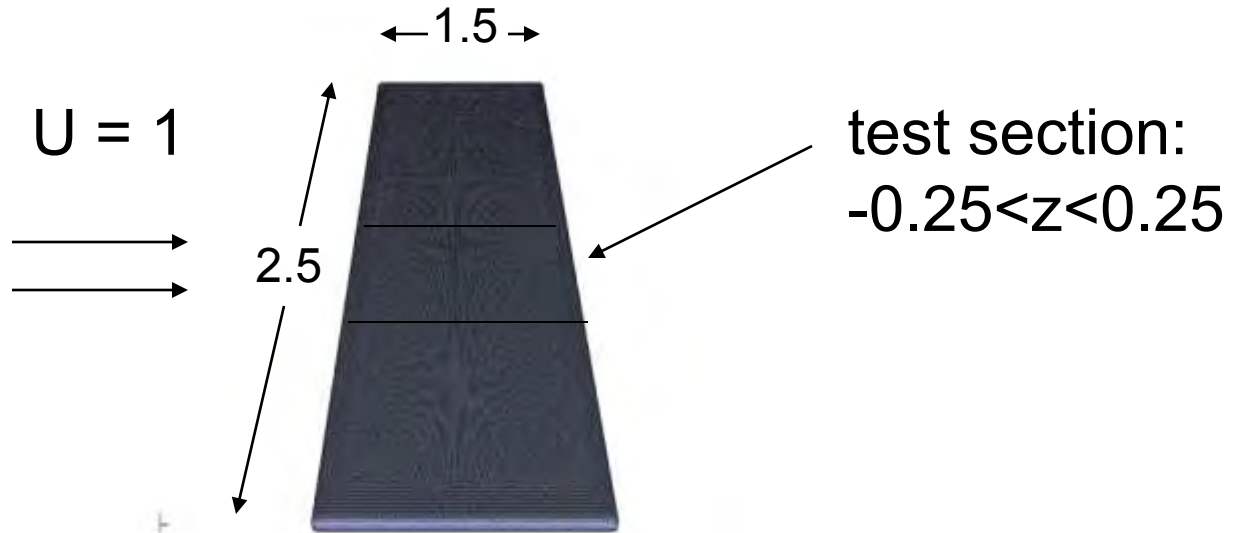
**Vortex lattice  
(response to  
lateral perturbation)**



**Oblique roller vortices &  
partial pairing (response to  
upstream turbulence).**

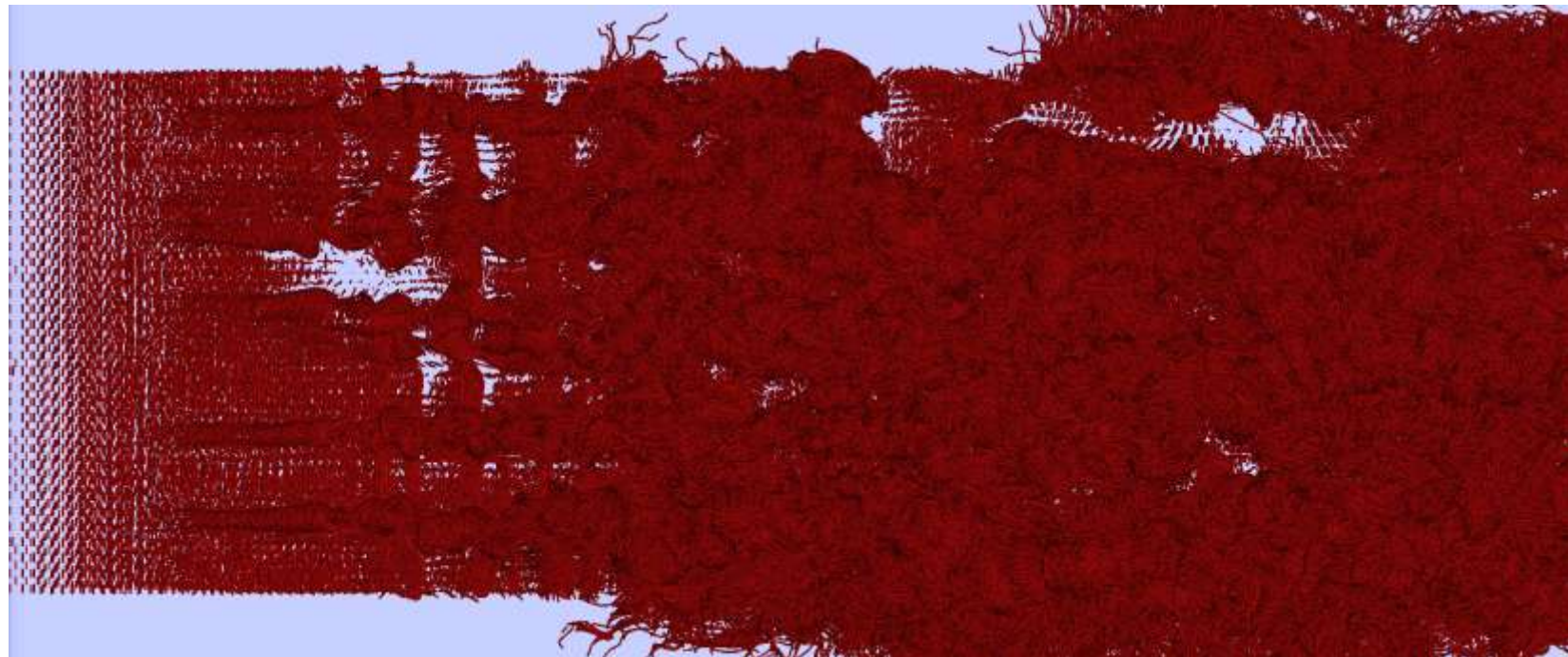
# Boundary Layer

# Boundary Layer Simulations



**62,272 surface triangles,  
684,992 prisms,  
22,000,000 vortex tubes  
Re = 50,000, 80,000**

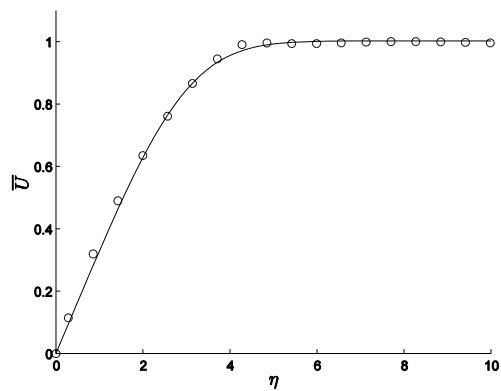
**74,274 surface triangles,  
817,014 prisms,  
28,000,000 vortex tubes  
Re = 80,000**



L

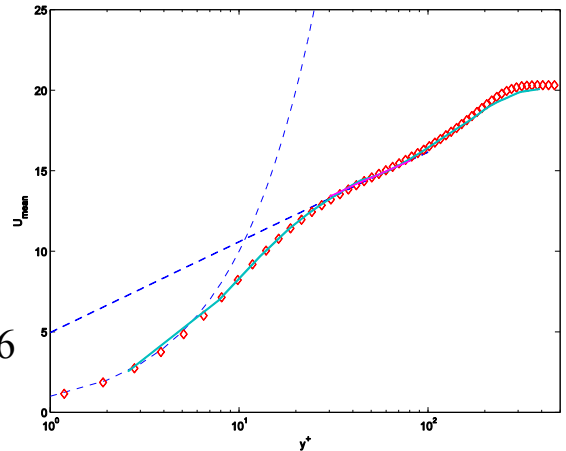
# Mean Velocity Predictions

$$\overline{U}^+ = y^+$$

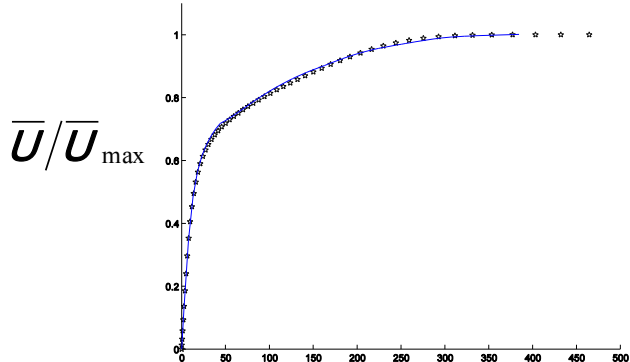


Blasius BL

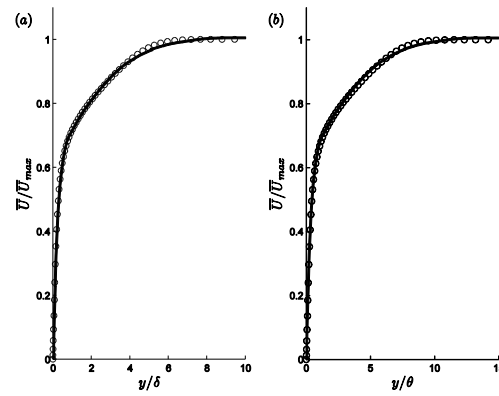
$$\overline{U}^+ = \frac{1}{0.437} \ln(y^+) + 5.66$$



Computed  $U^+$  ( $R_\theta = 670$ ) vs.  
Spalart DNS ( $R_\theta = 670$ ).

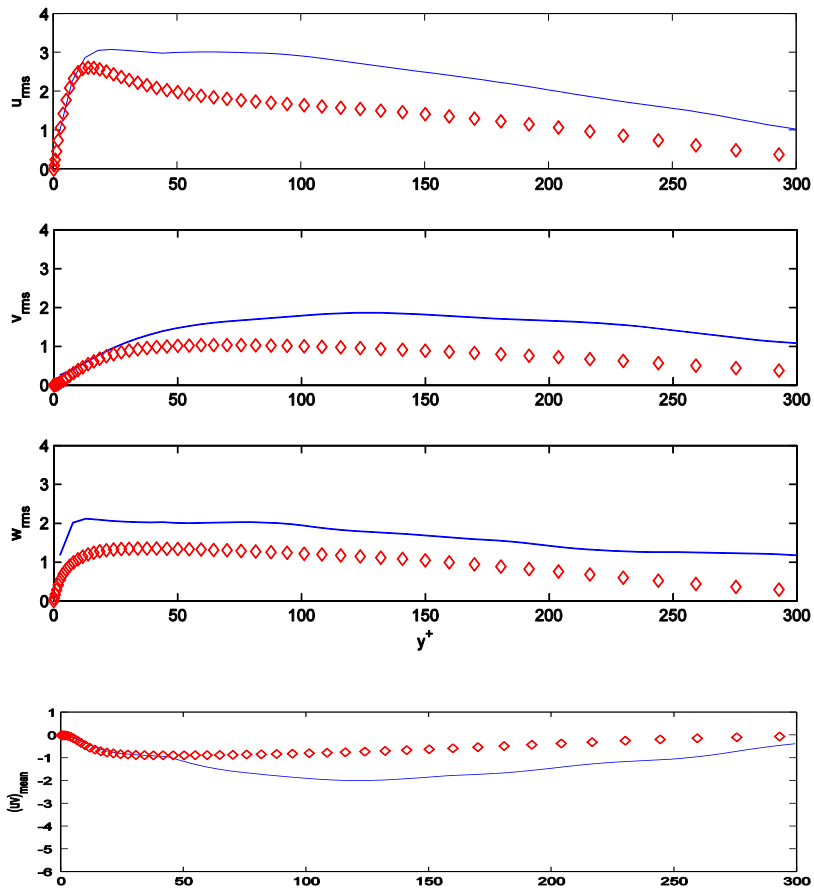


$$y^+$$



Scaling with  $\delta$  and  $\theta$

# Reynolds Stresses





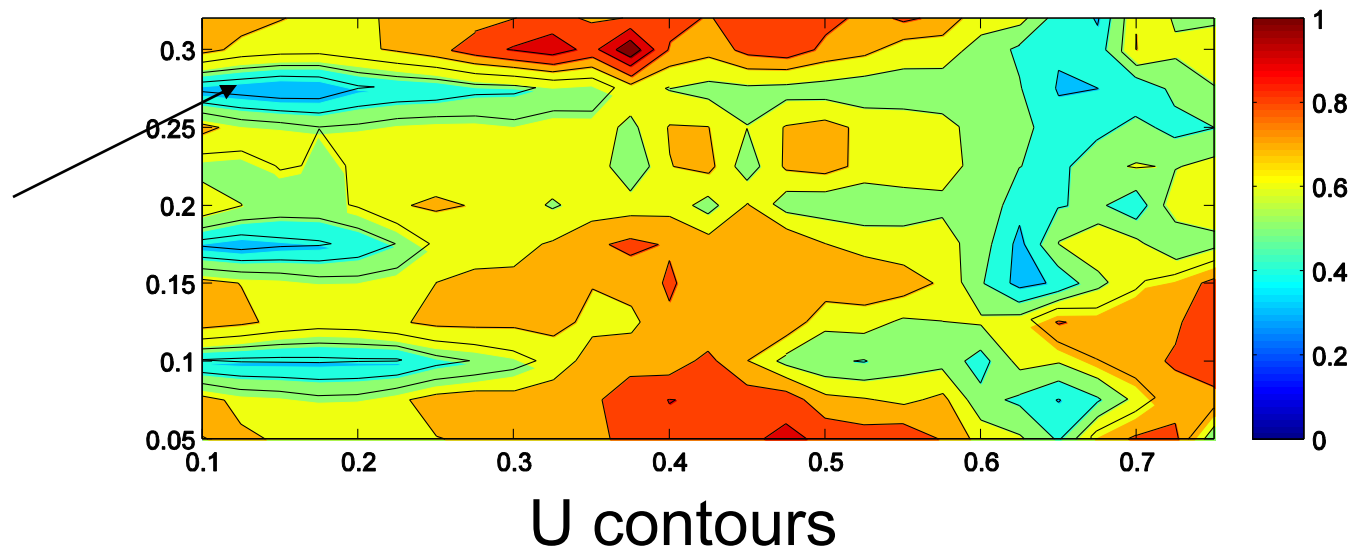
Transition is dominated by the appearance of vortex furrows - spaced approximately at the boundary layer thickness.

Vortex furrows override low speed streaks.

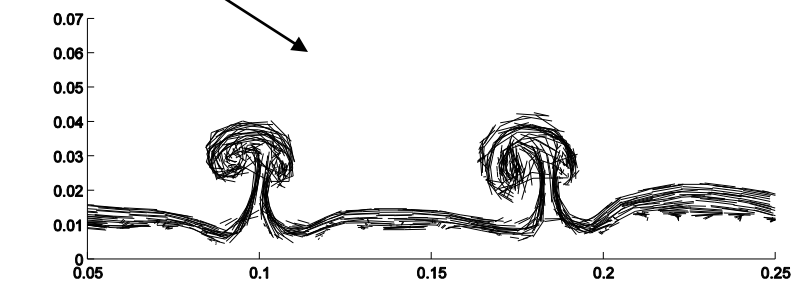
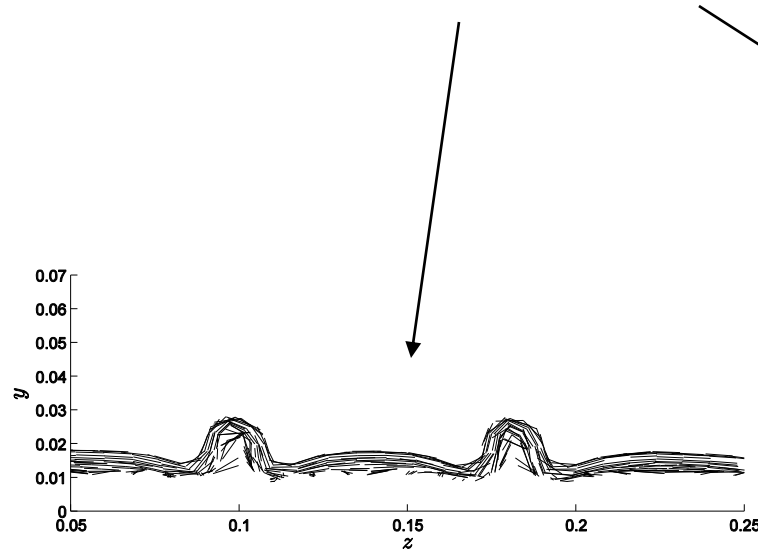
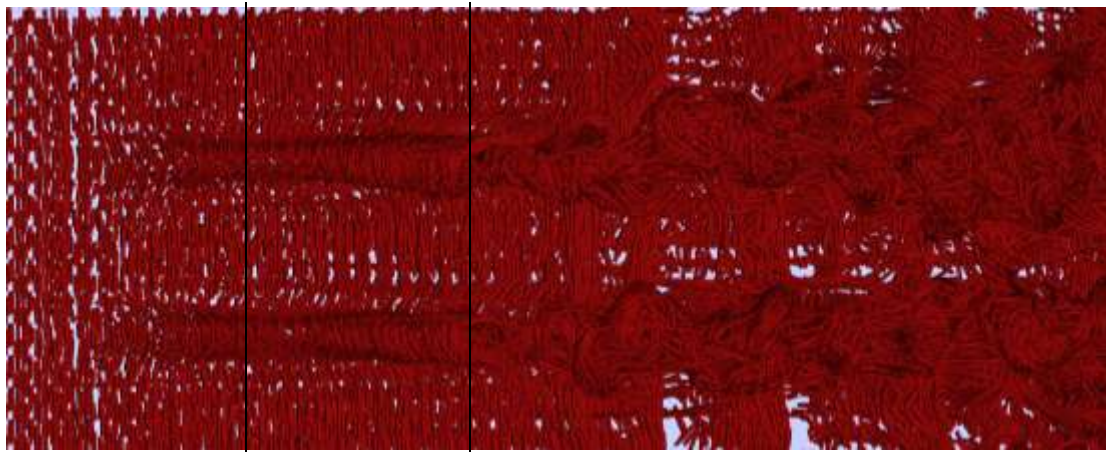
Vortex  
furrows



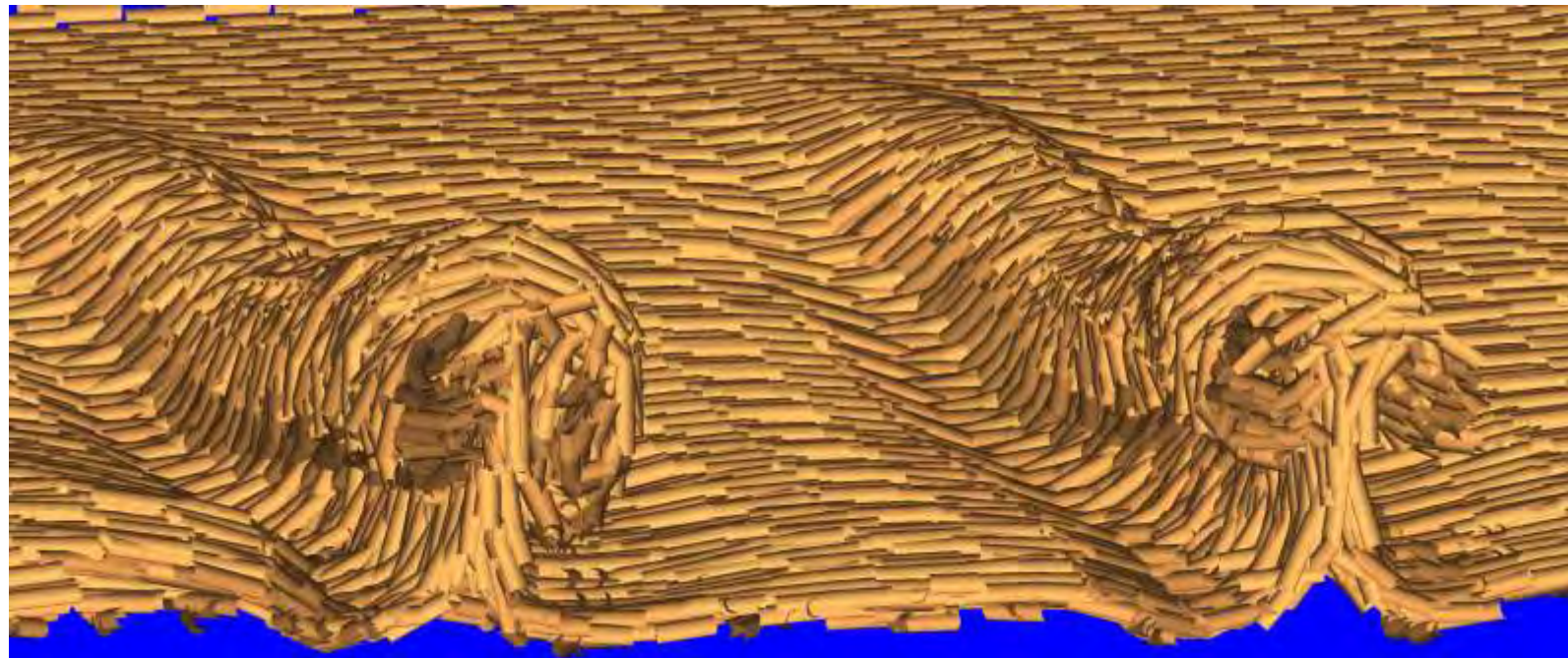
Low speed  
streaks

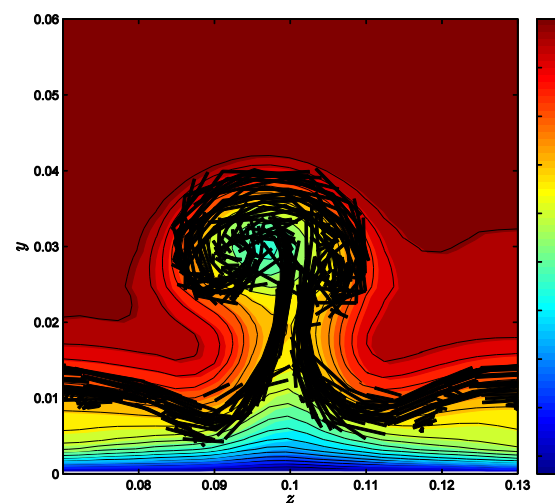
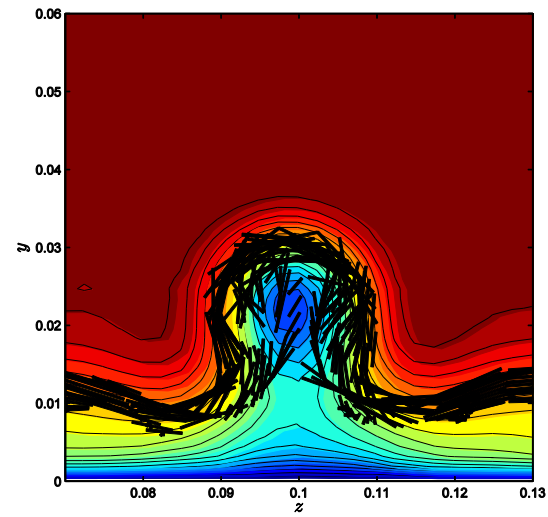
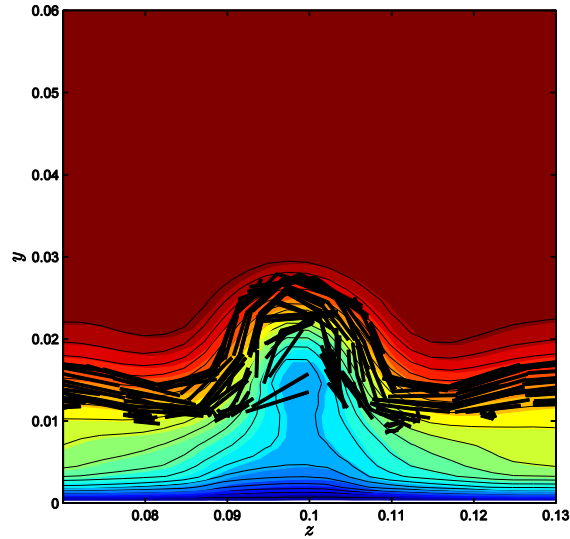


# Transverse cuts through the furrows.

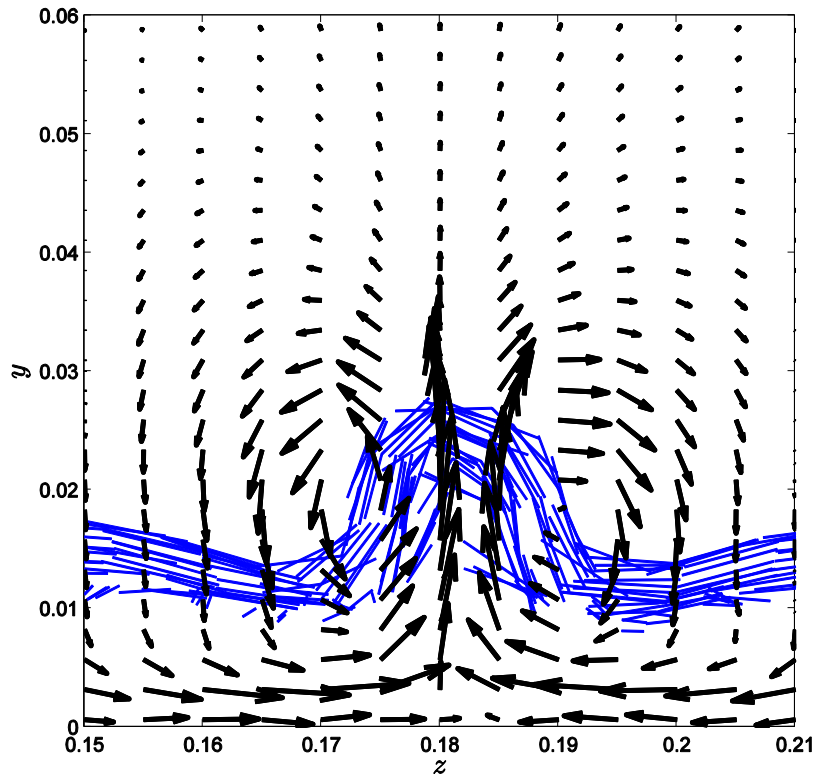


Vortex furrows erupting into mushroom-shaped filaments

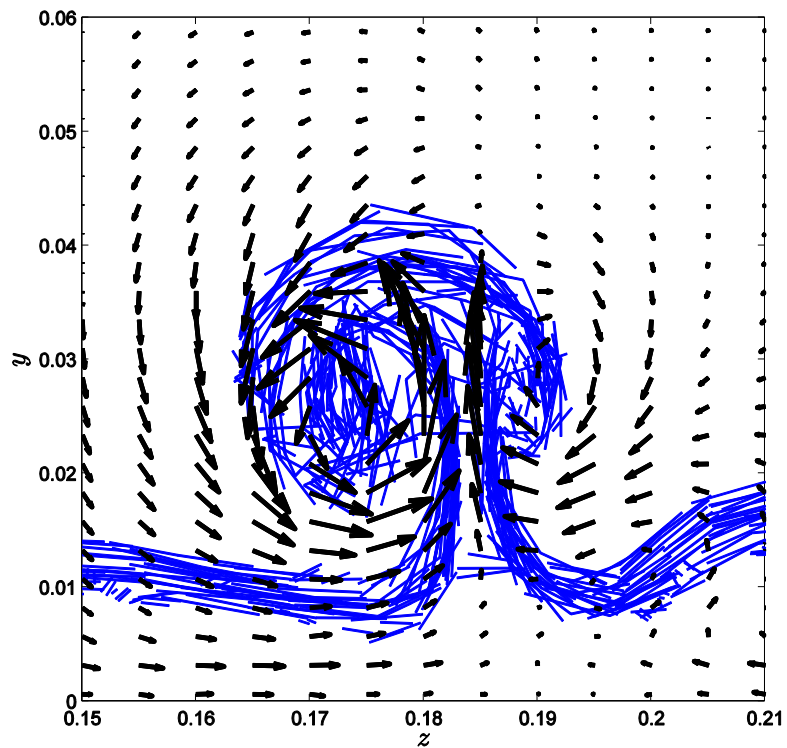




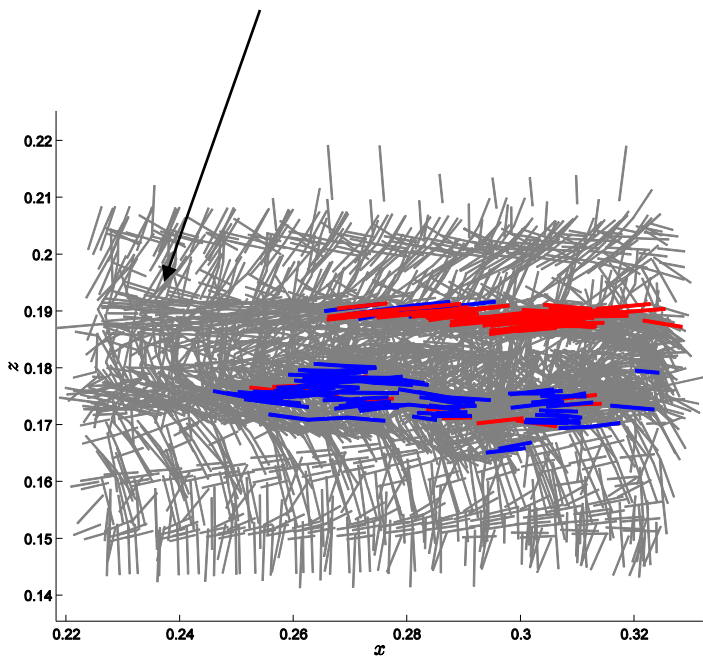
Ejection of low speed fluid.



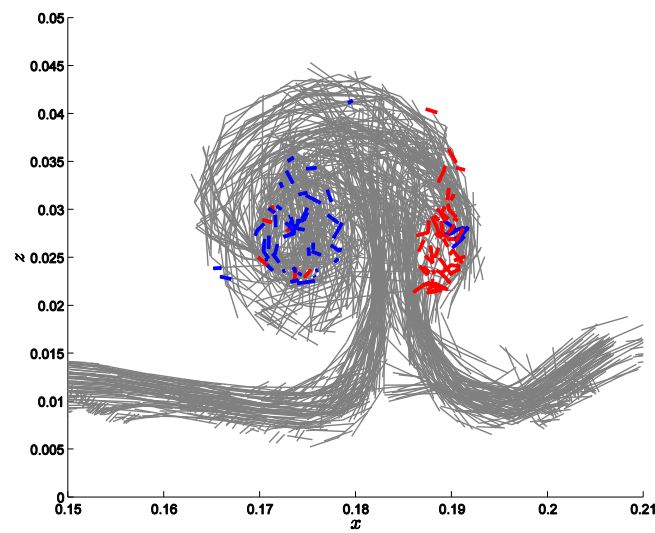
Counter-rotating motion is associated with the uplifted filaments in the furrows.



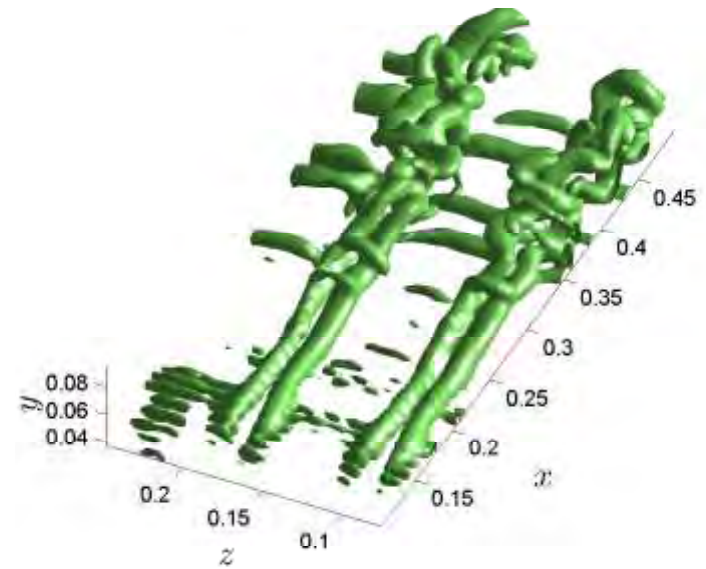
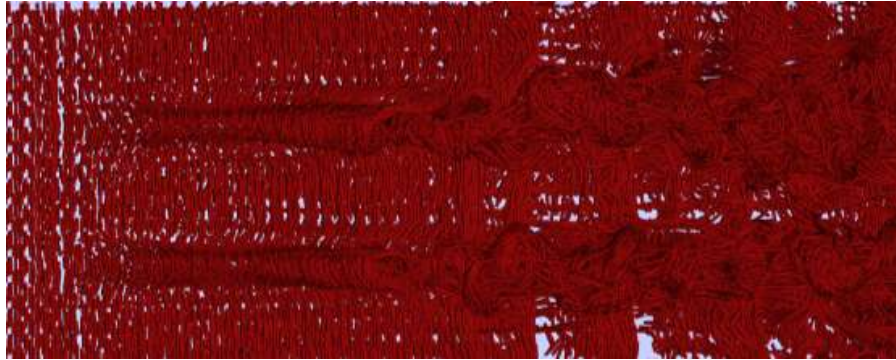
**Initially the counter-rotating motion is produced by forward tilted filaments in the arches: there are no streamwise filaments.**



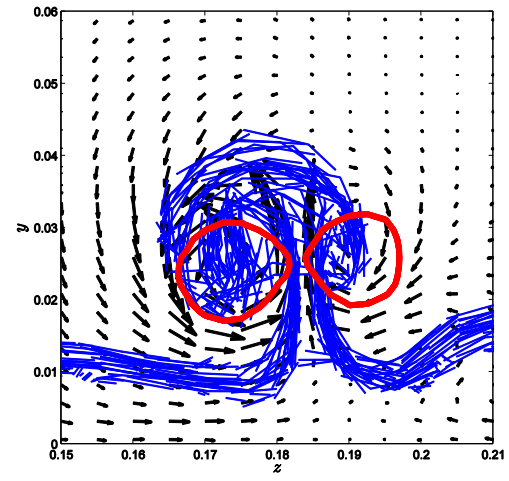
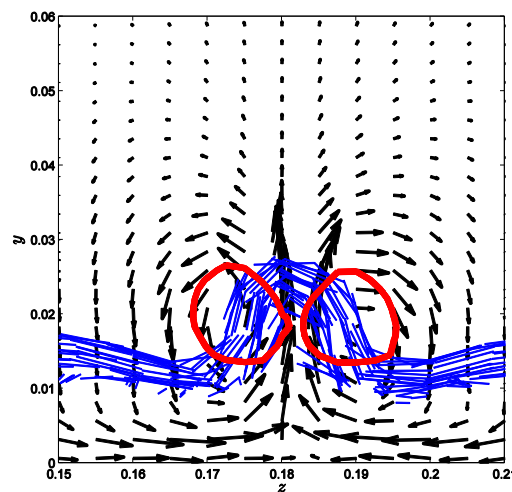
**True streamwise vorticity is prevalent in the lobes of the mushroom profile,**



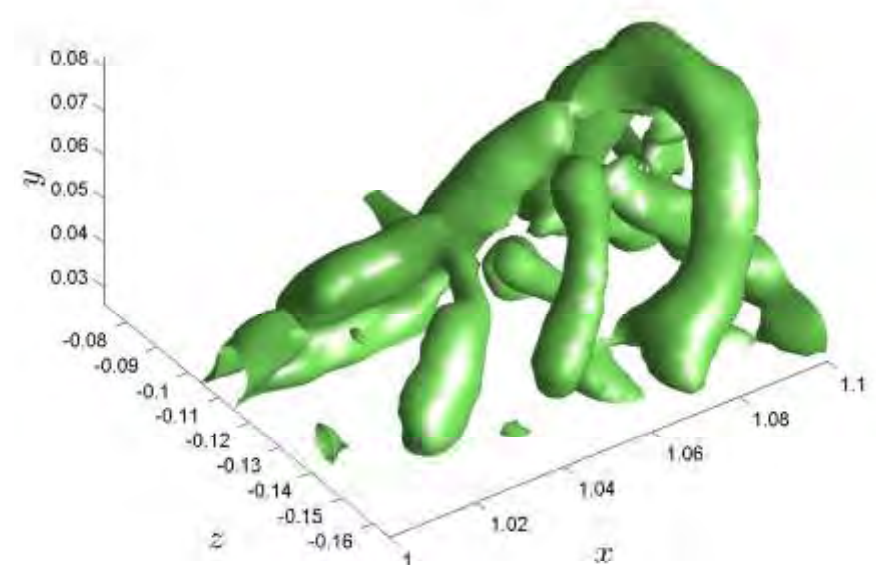
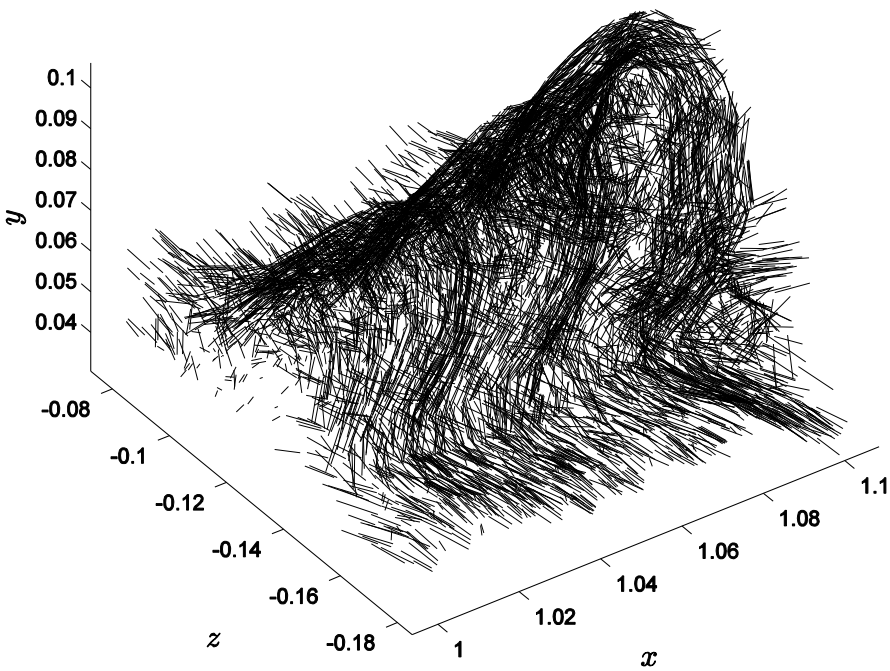
**When viewed as isocontours of rotational motion (2nd eigenvalue of  $S^2+W^2$ ), the furrows have the appearance of hairpin vortices.**



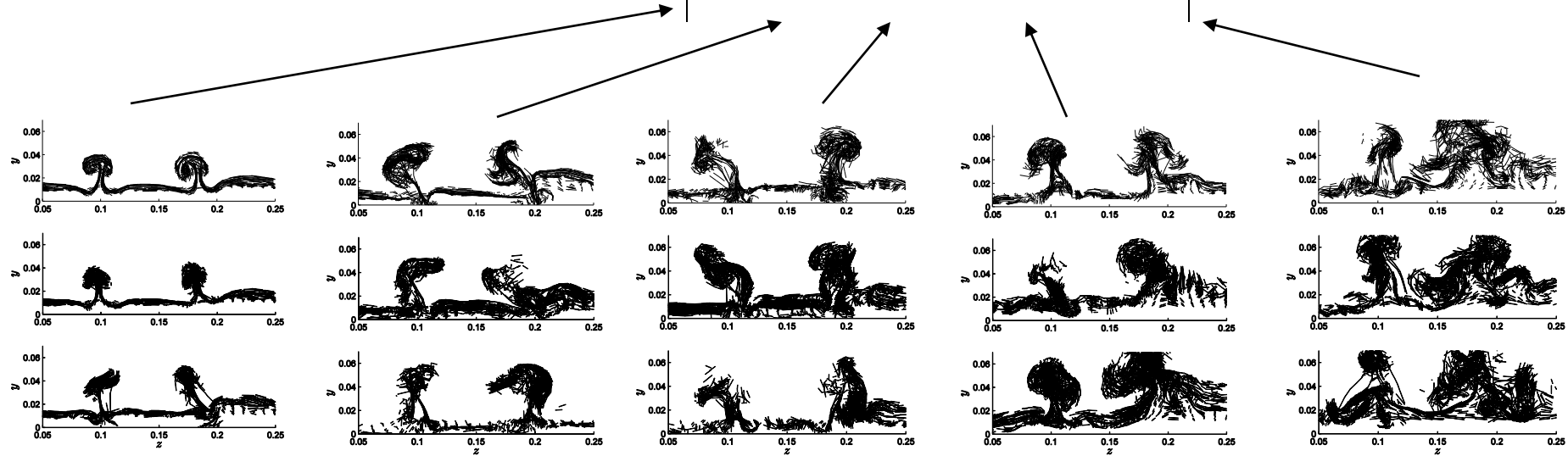
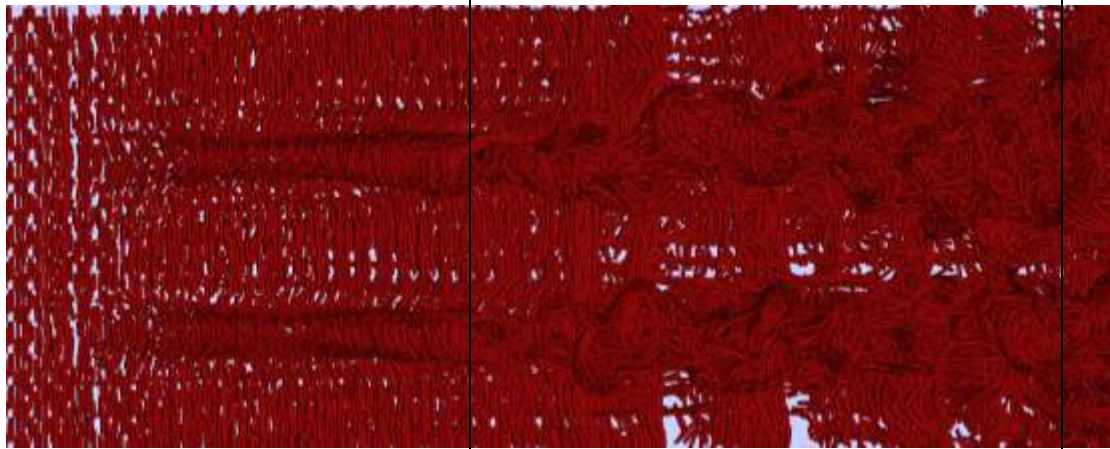
**Isocontours (shown in red) representing the "legs of hairpin vortices mark the counter-rotating motion associated with the furrows.**



Shear roll-up of spanwise vorticity is the apparent source of arch-type vortices that straddle the furrows.



# Breakdown of furrows into turbulence



# Ground Vehicle Flows

# Ahmed body

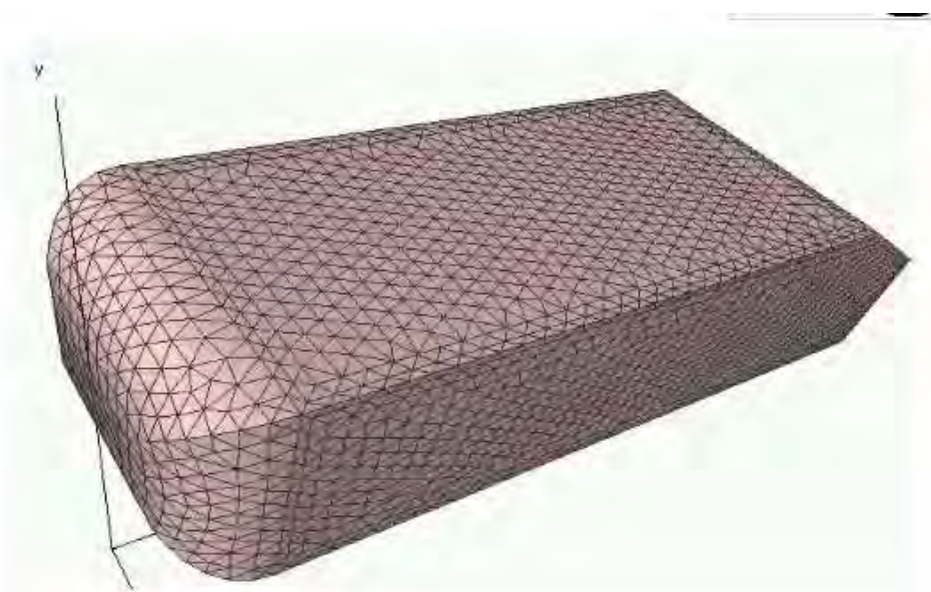
12.5, 25, 30 degree base slant angle

$R_e=500,000$

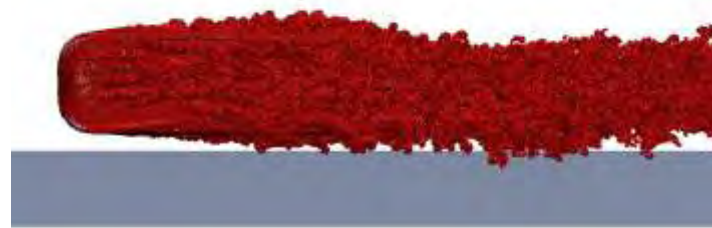
Inviscid ground plane

Front:  $x=0$

Back:  $x=1$



# Ahmed Body with 30° base slant angle



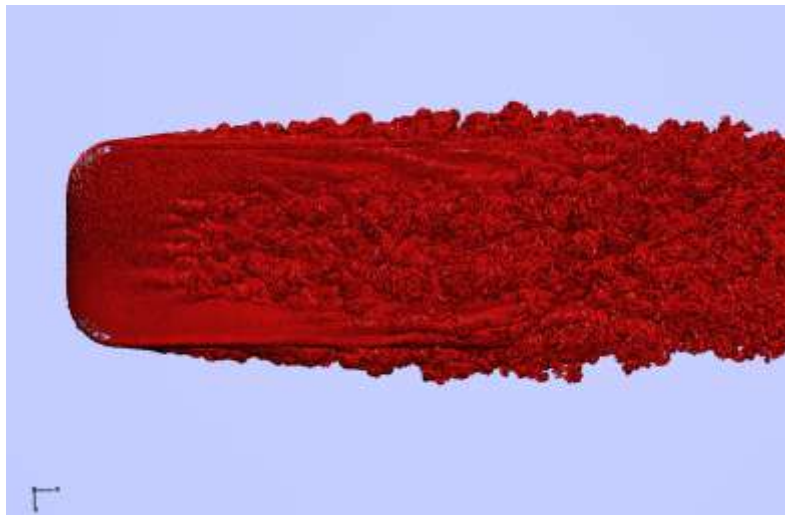
L

Side



L

Front



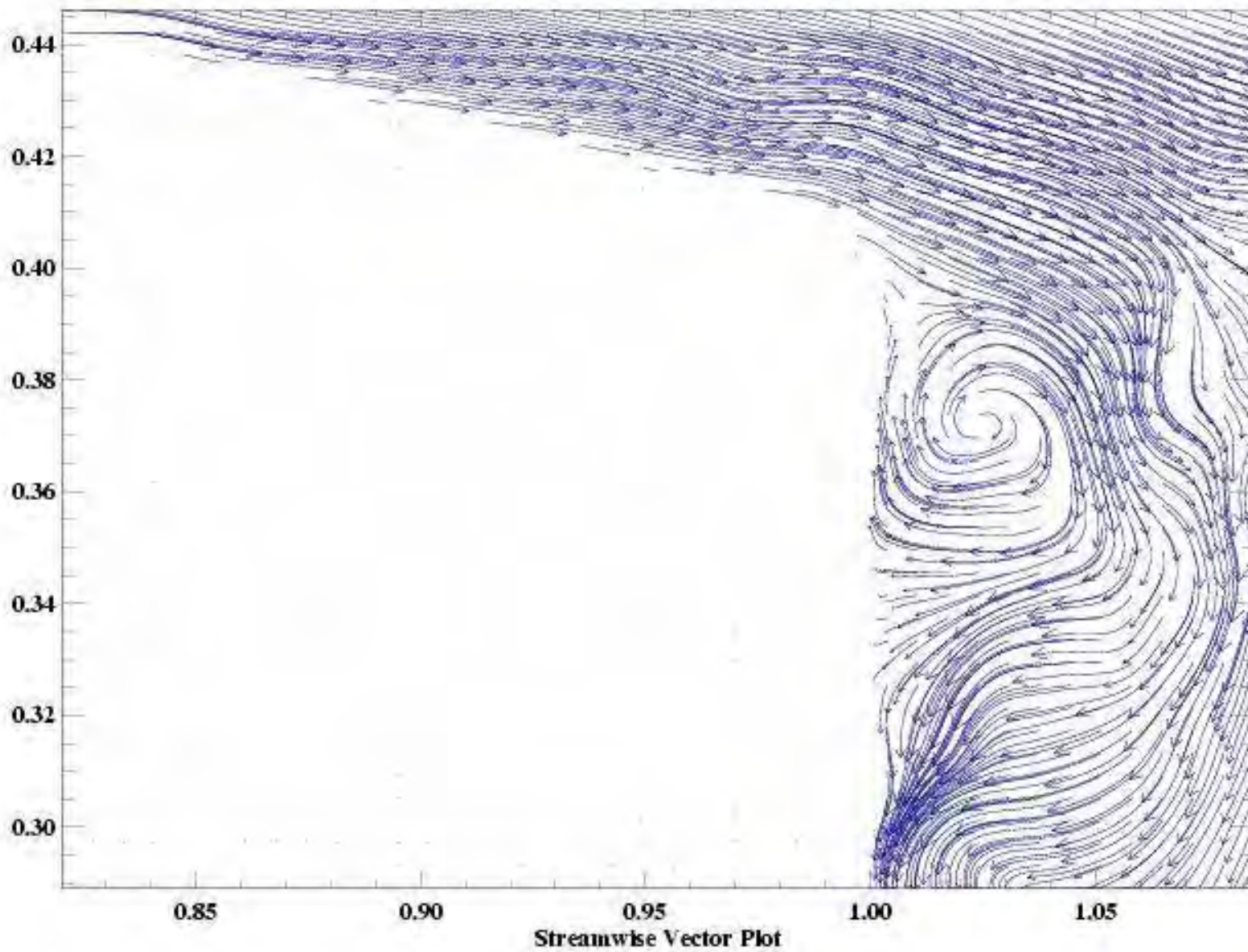
F

Top

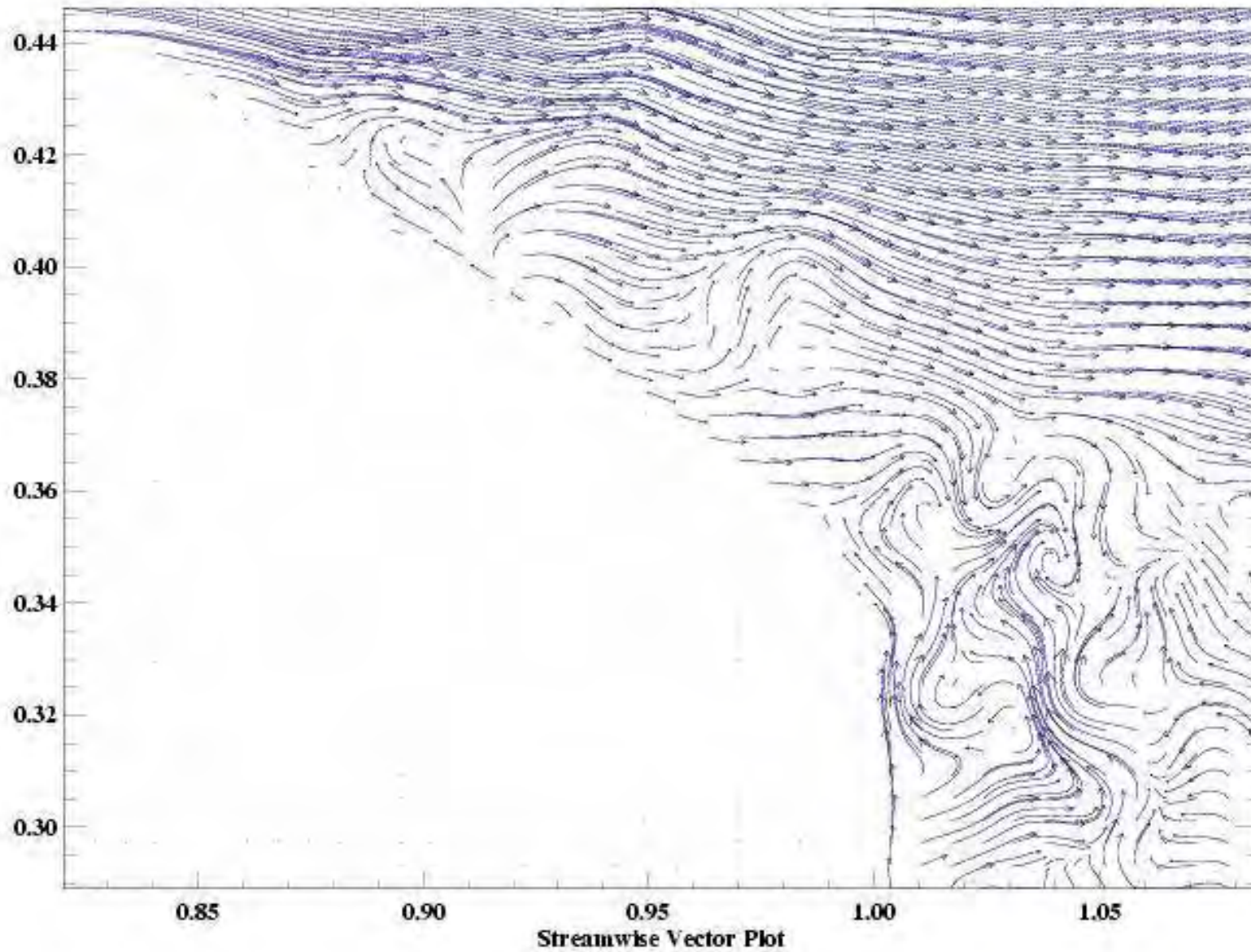


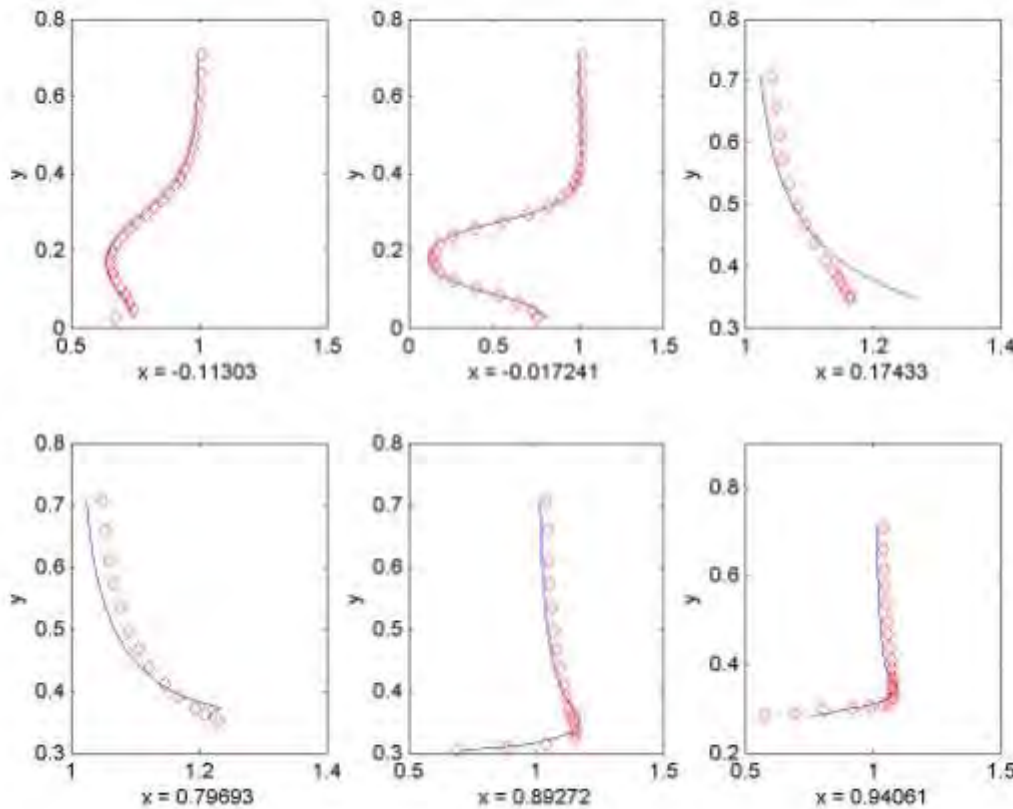
Rear during startup

# Ahmed Body with 12.5° base slant angle

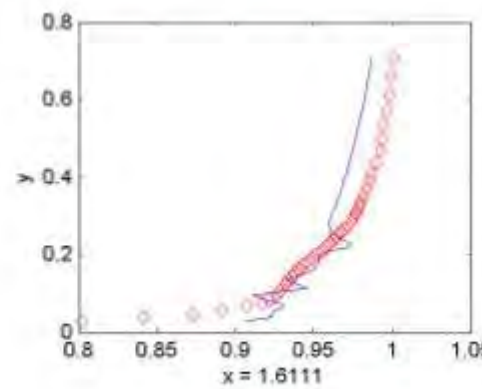
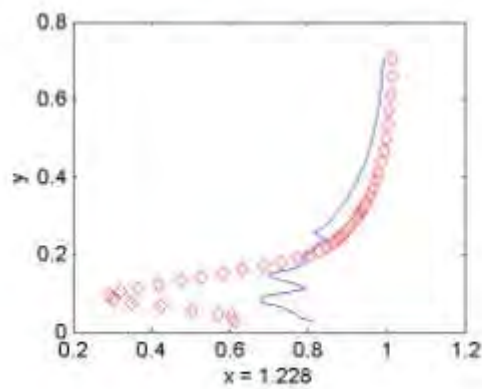
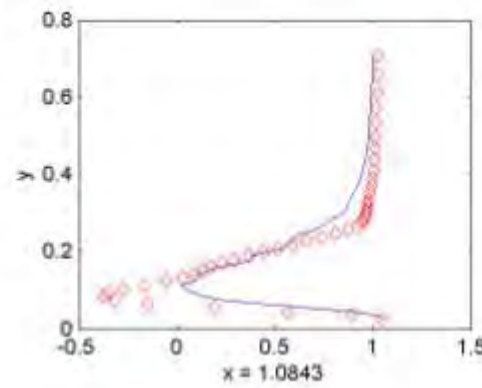
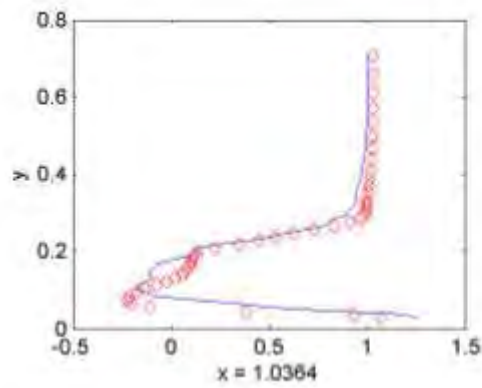


# Ahmed Body with 30° base slant angle

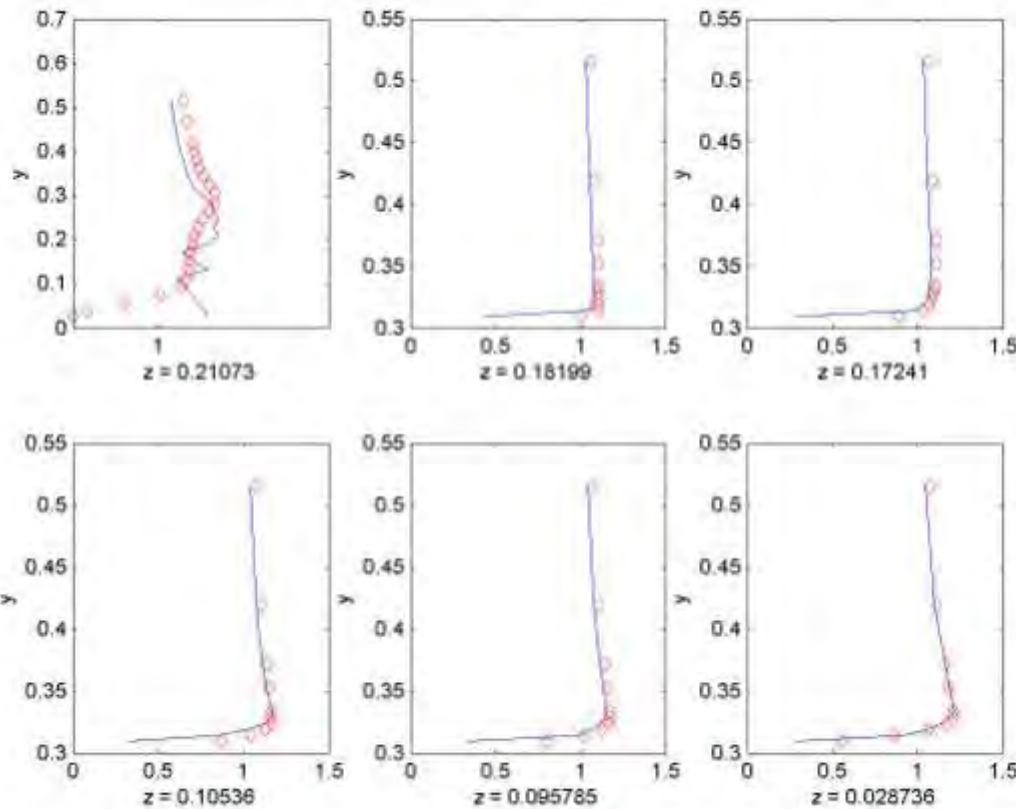




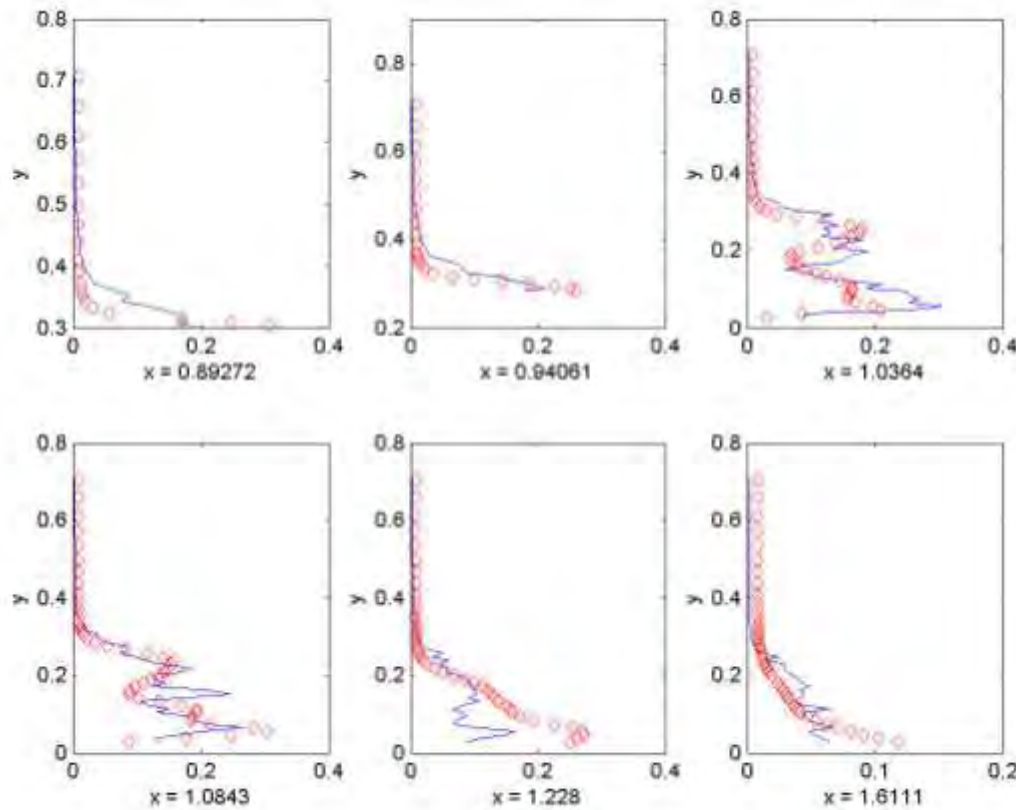
U on centerline.



U in wake.



$U$  on window,  $x = 0.8678$ .



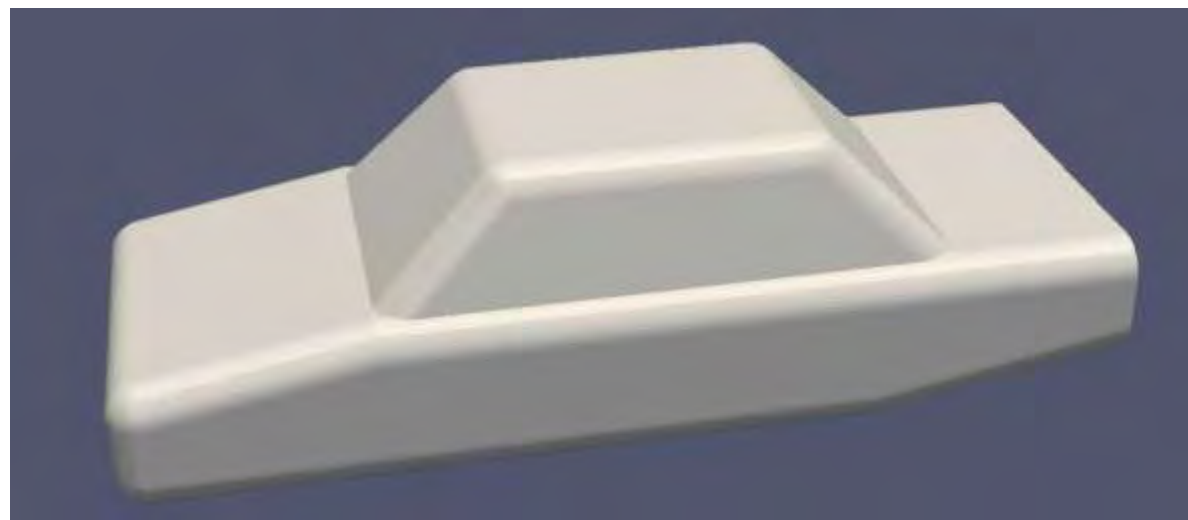
K on centerline and wake.

## **MIRA Vehicle**

**Re=500,000**

**Inviscid ground plane, or**

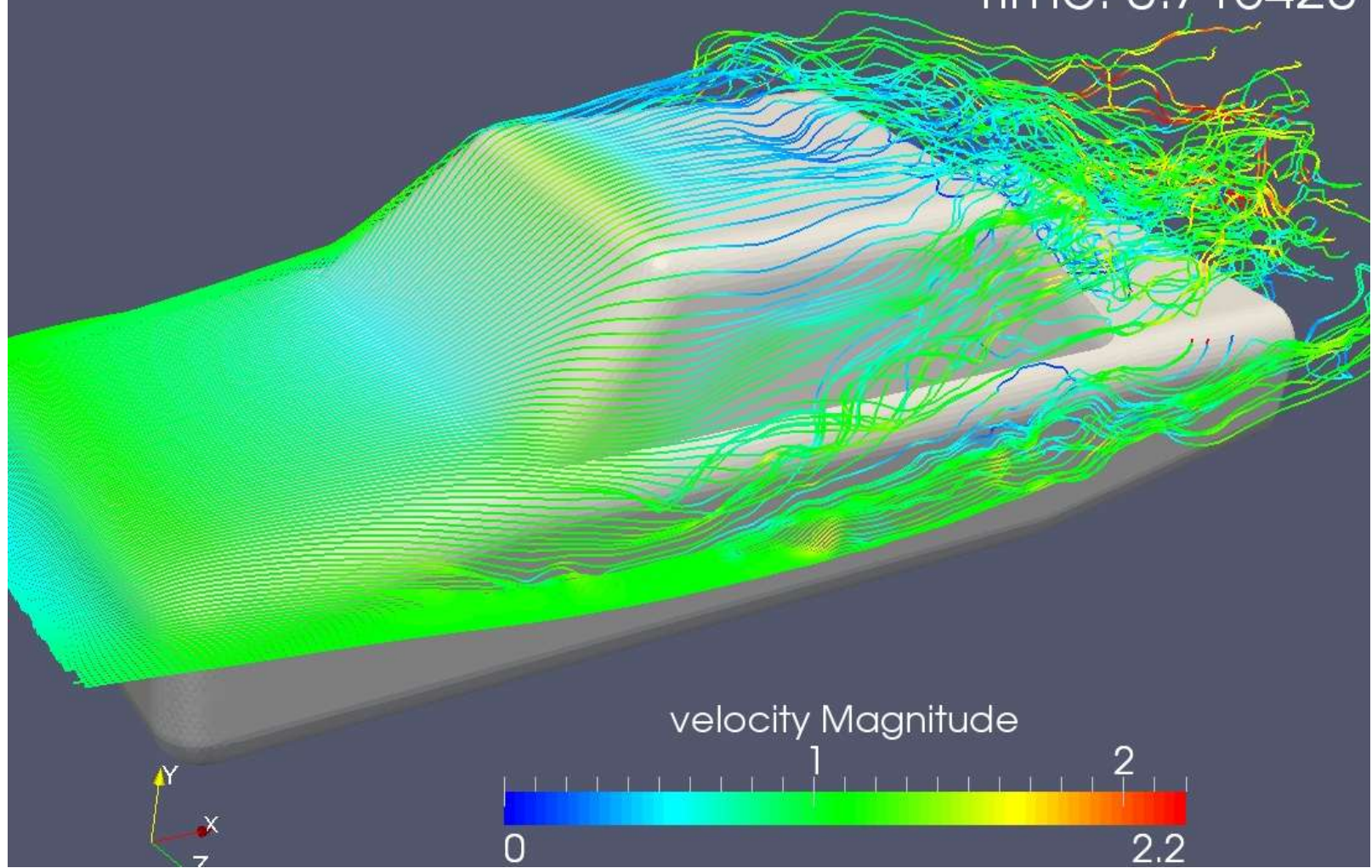
**Moving, viscous ground plane**

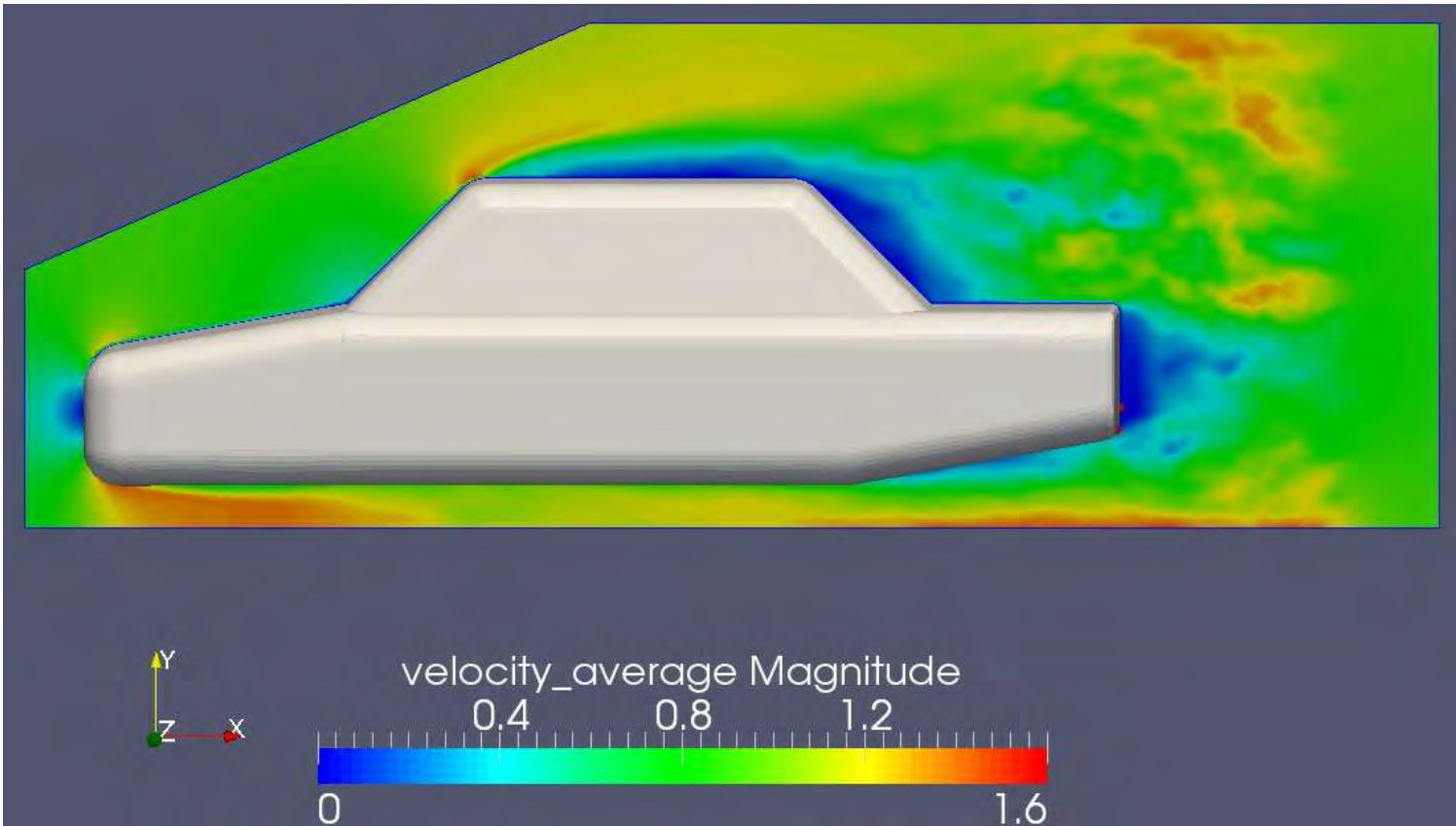




L

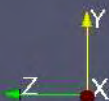
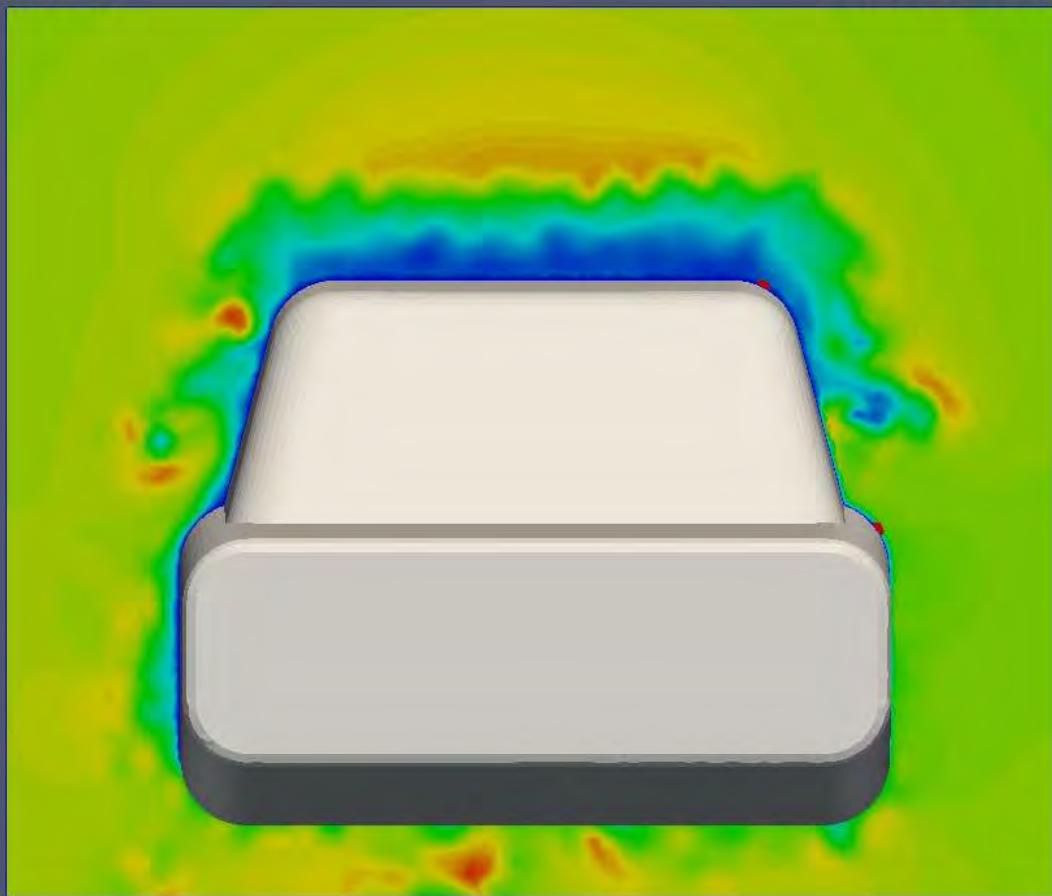
Time: 0.716420



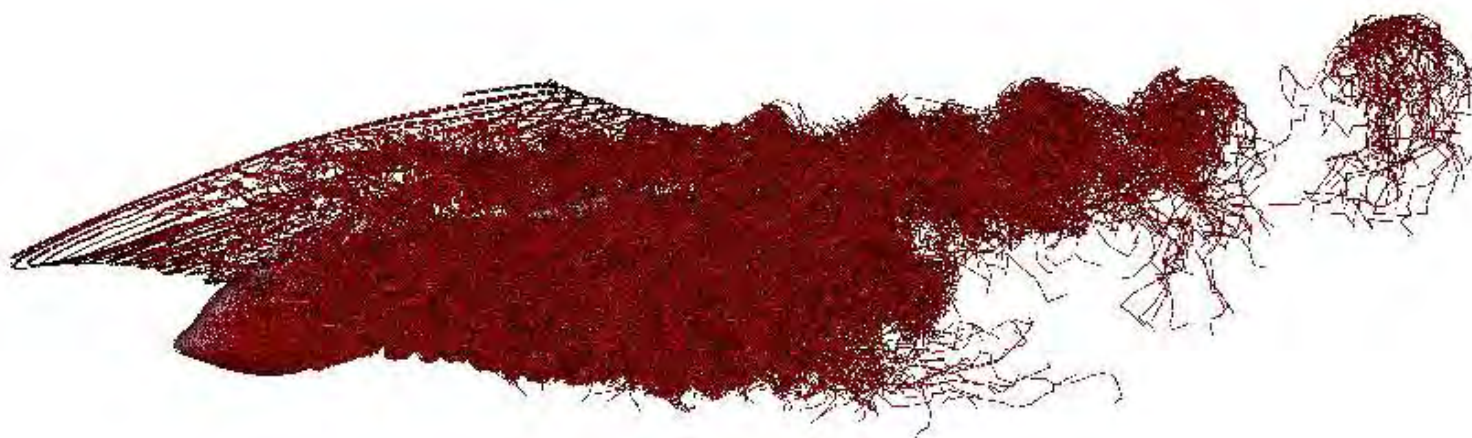


Back View

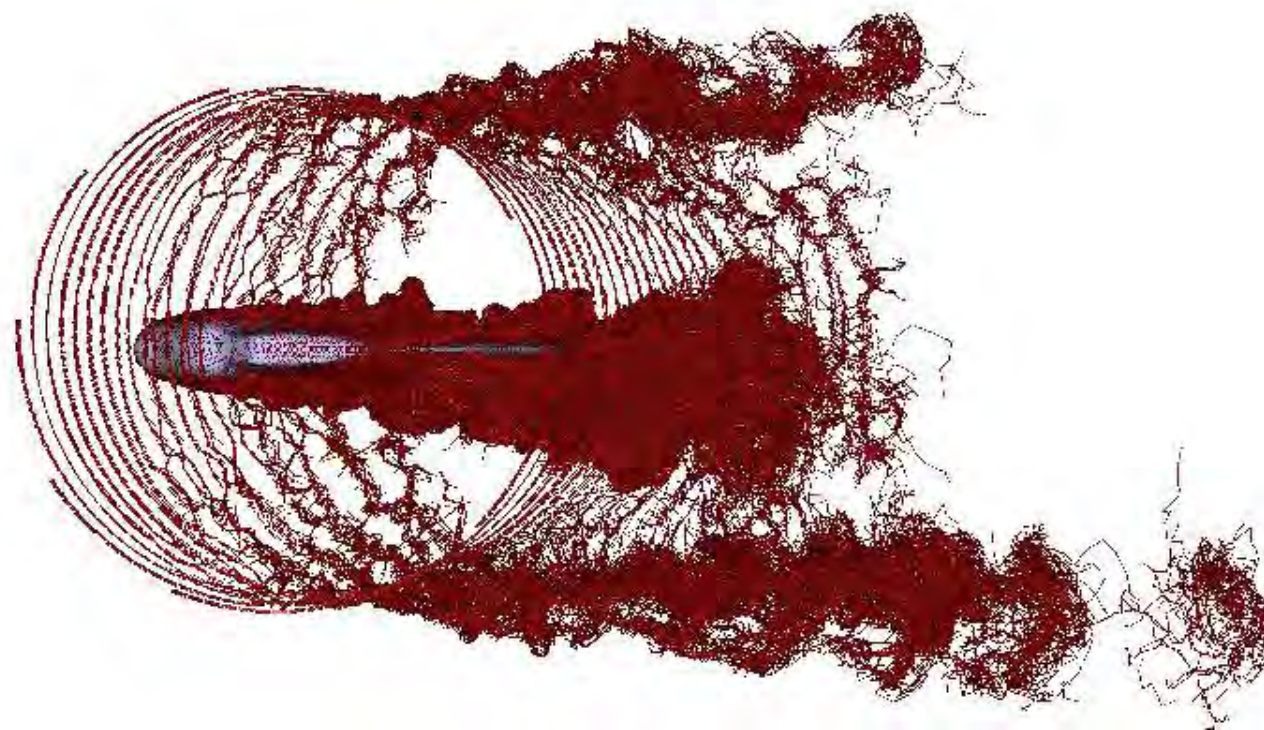
Time: 0.215900

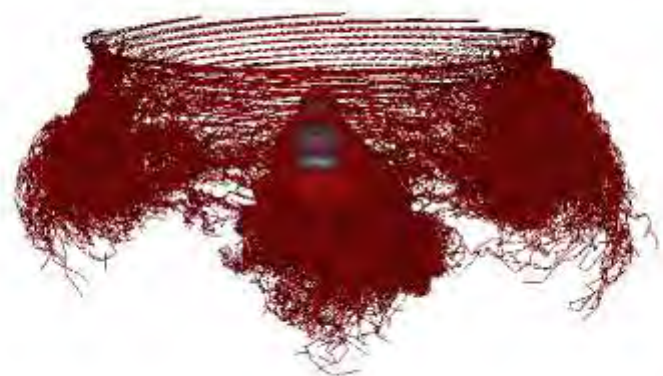


# Rotorcraft Simulations

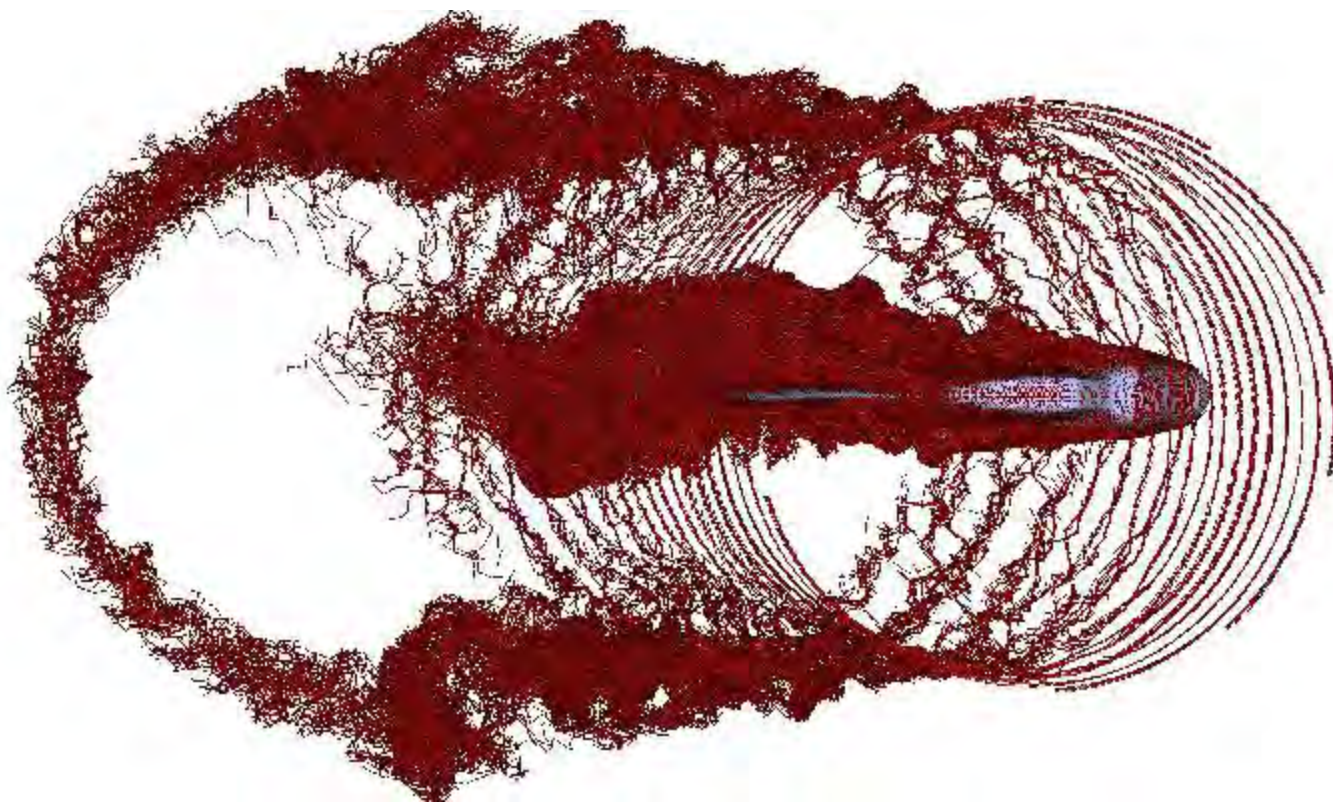


—

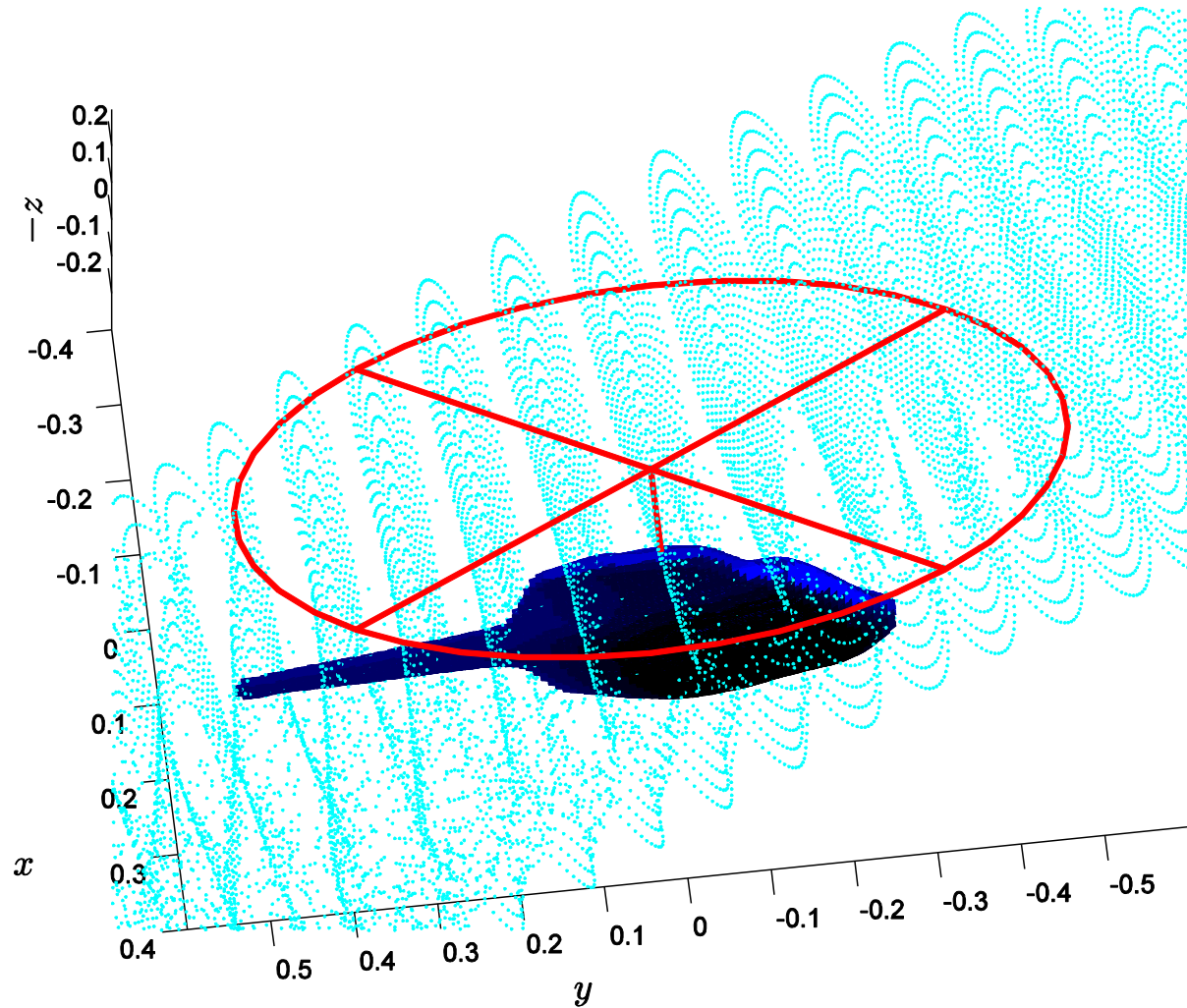


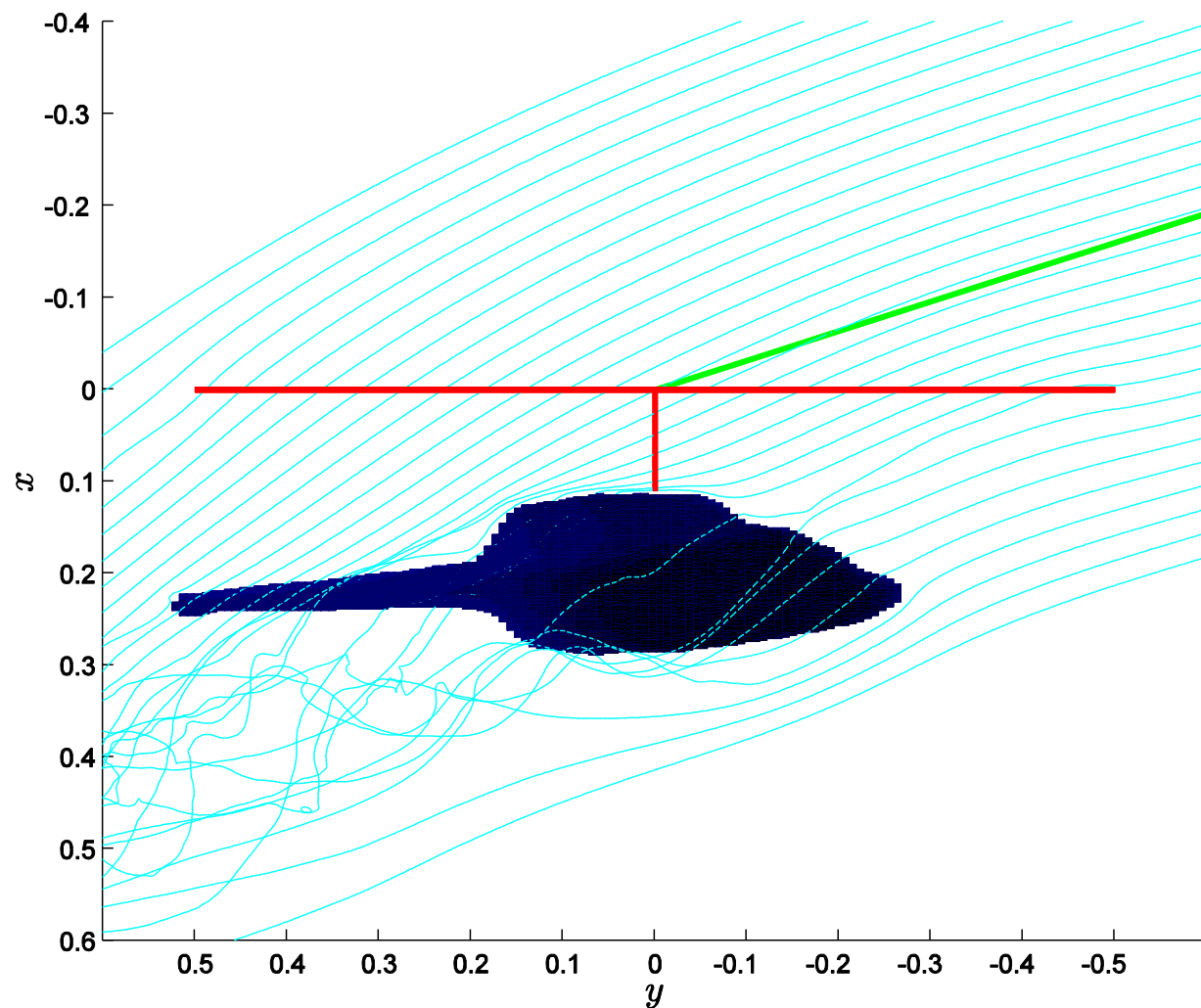


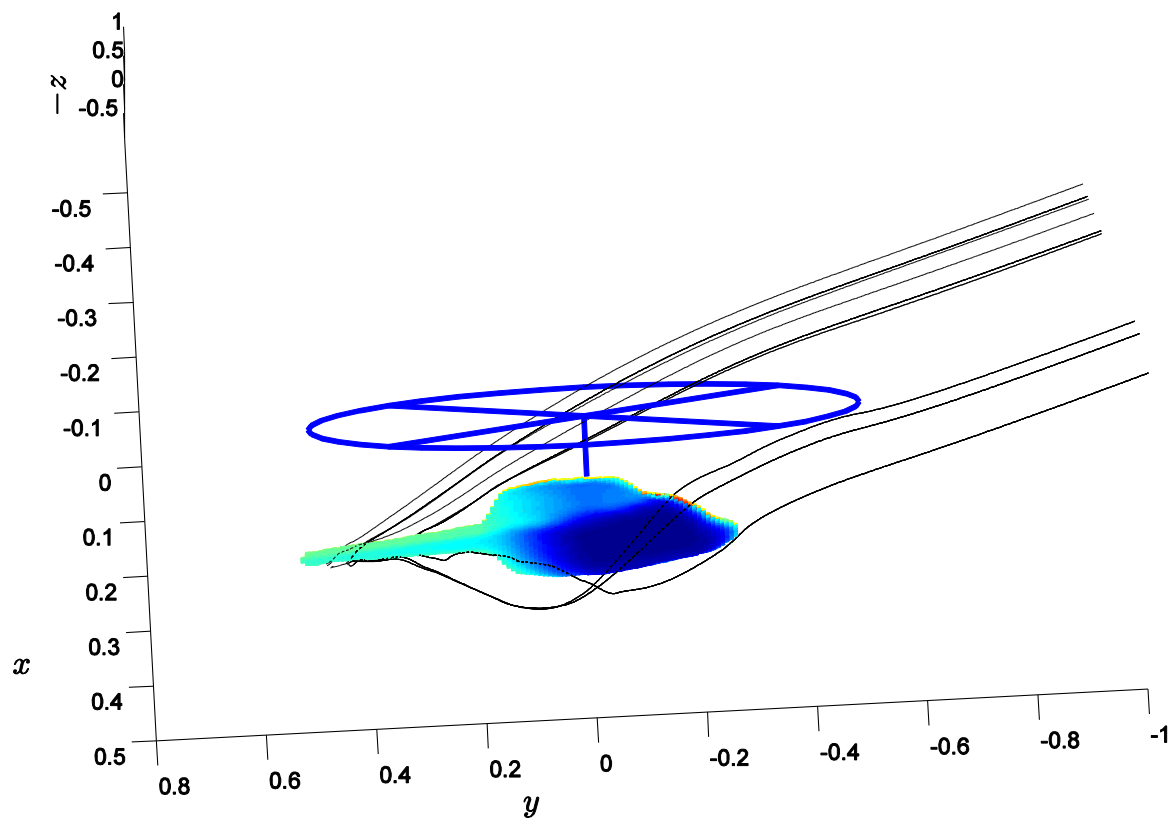
Γ



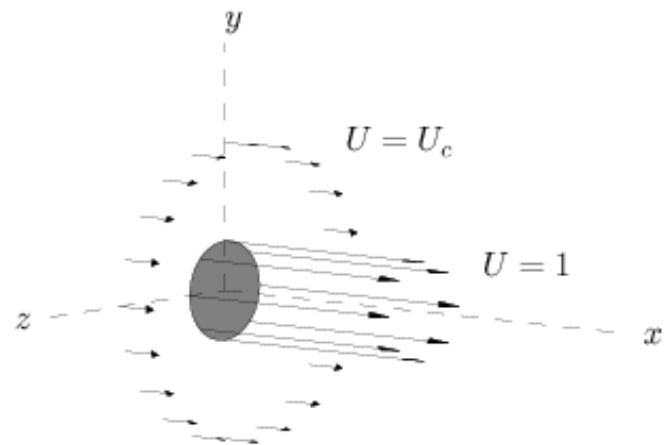
L







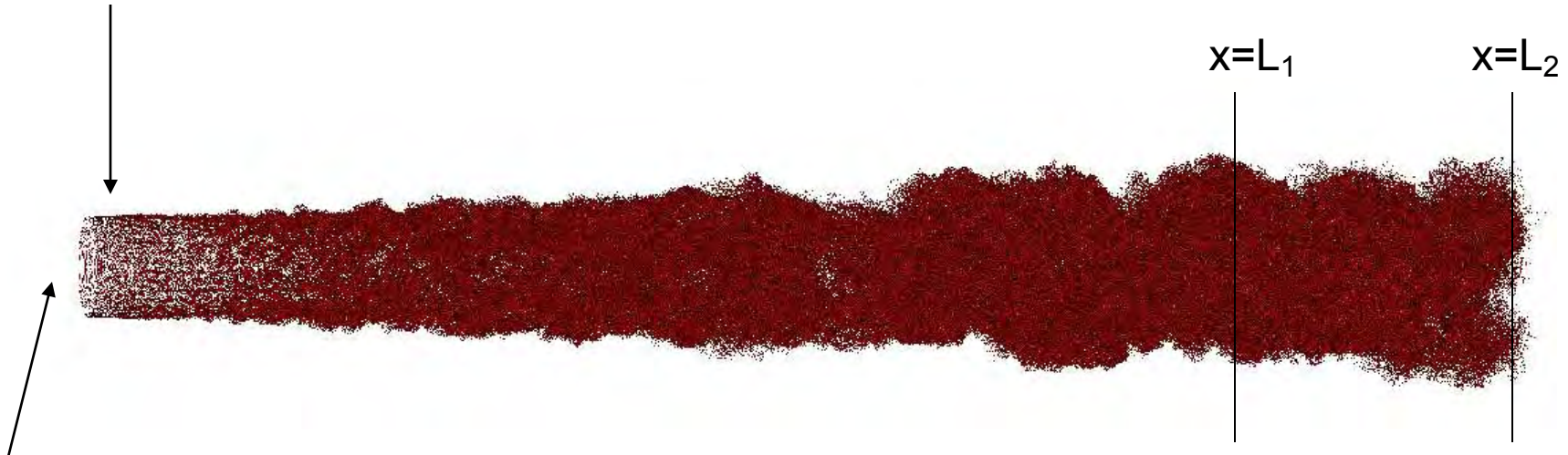
# Coflowing Round Jet



# Co-flowing Round Jet

Coflows = 1/2, 1/3, 1/4, 1/5, 1/10.

5 vortex rings at unit diameter orifice.



Potential flow:  
disk shaped source  
maintains unit  
velocity at inlet

- (a) Remove rings when  $> L_1$   
**or**
- (b) Remove rings if any part  $> L_2$

## Co-flowing Round Jet

$U_c$	$h$	BC	$L/d$
1/10	0.055	a	5.25
1/5	0.04	a	6.65
1/4	0.04	b	11.0
1/3	0.045	b	12.75
1/2	0.04	b	15.5

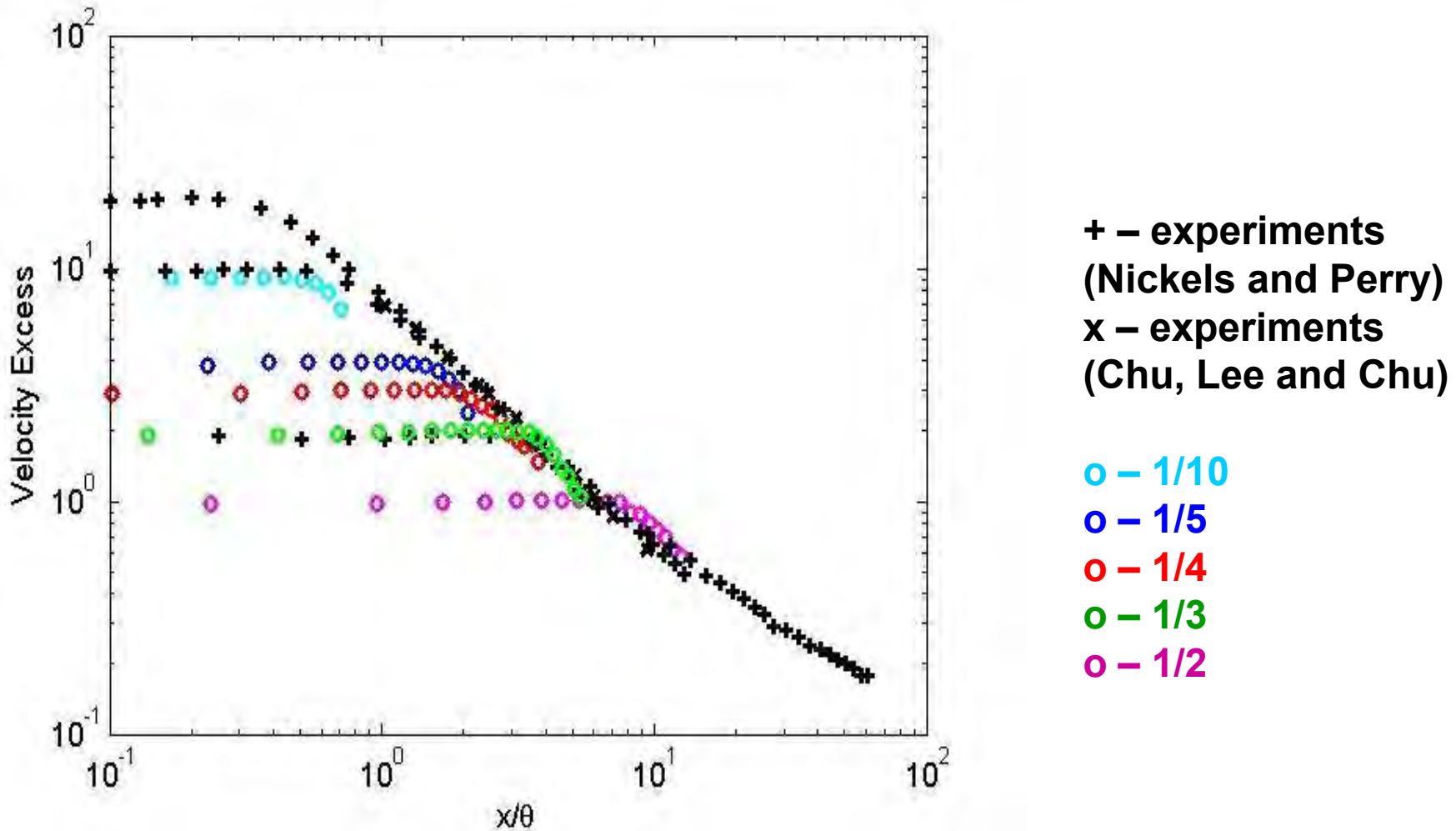
$$\theta \equiv \sqrt{2\pi \int \bar{U}(\bar{U} - U_c) r dr} / U_c \quad \theta \rightarrow \text{momentum thickness}$$

$$\delta \equiv \sqrt{\int (\bar{U} - U_c) r^2 dr} / \sqrt{\int (\bar{U} - U_c) dr}$$

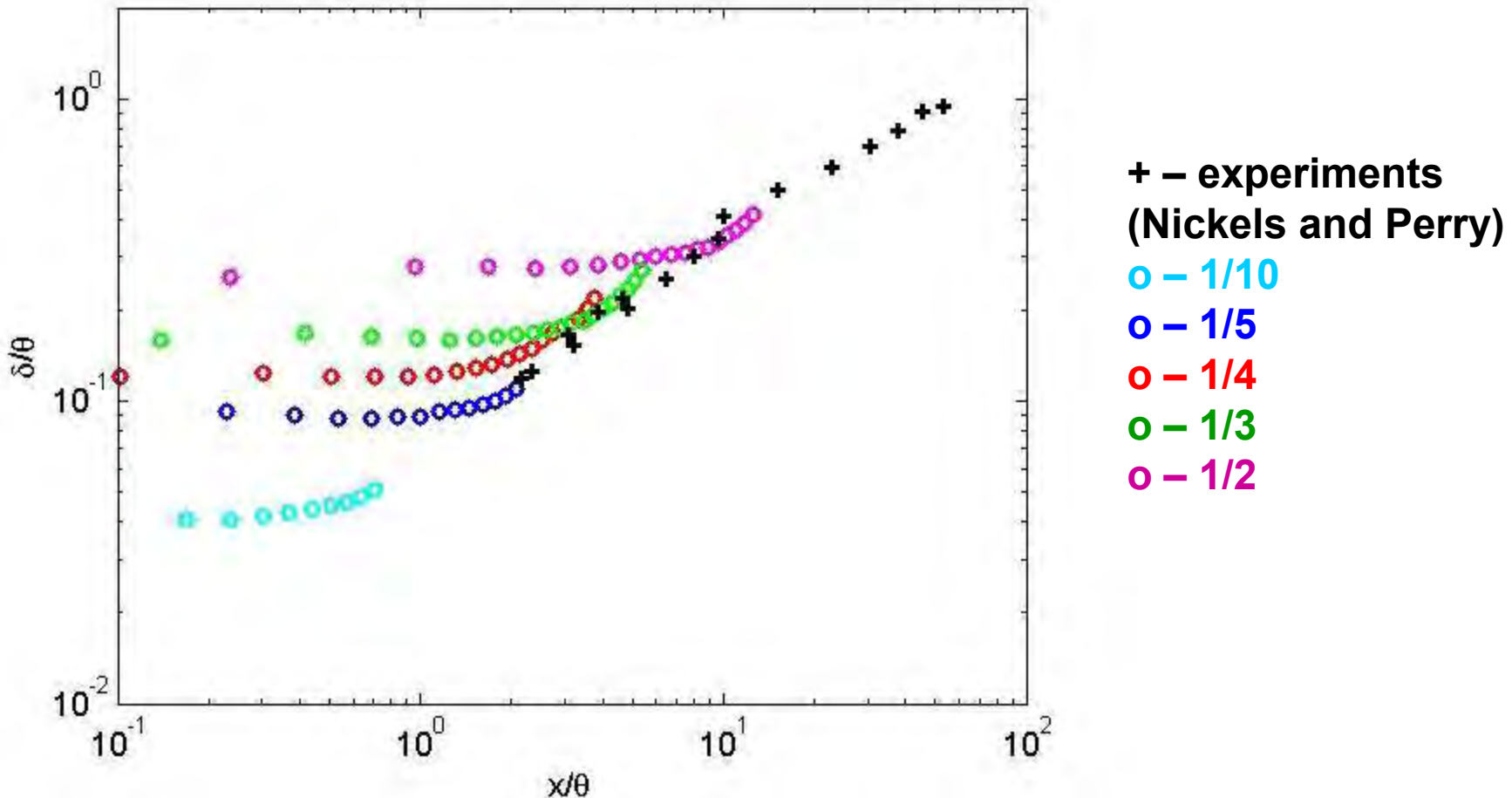
$$\bar{U}/U_0 = e^{-r^2/b^2} \quad b \rightarrow \text{Gaussian scale}$$

# Velocity Excess in Coflowing Round Jet vs. Streamwise Position

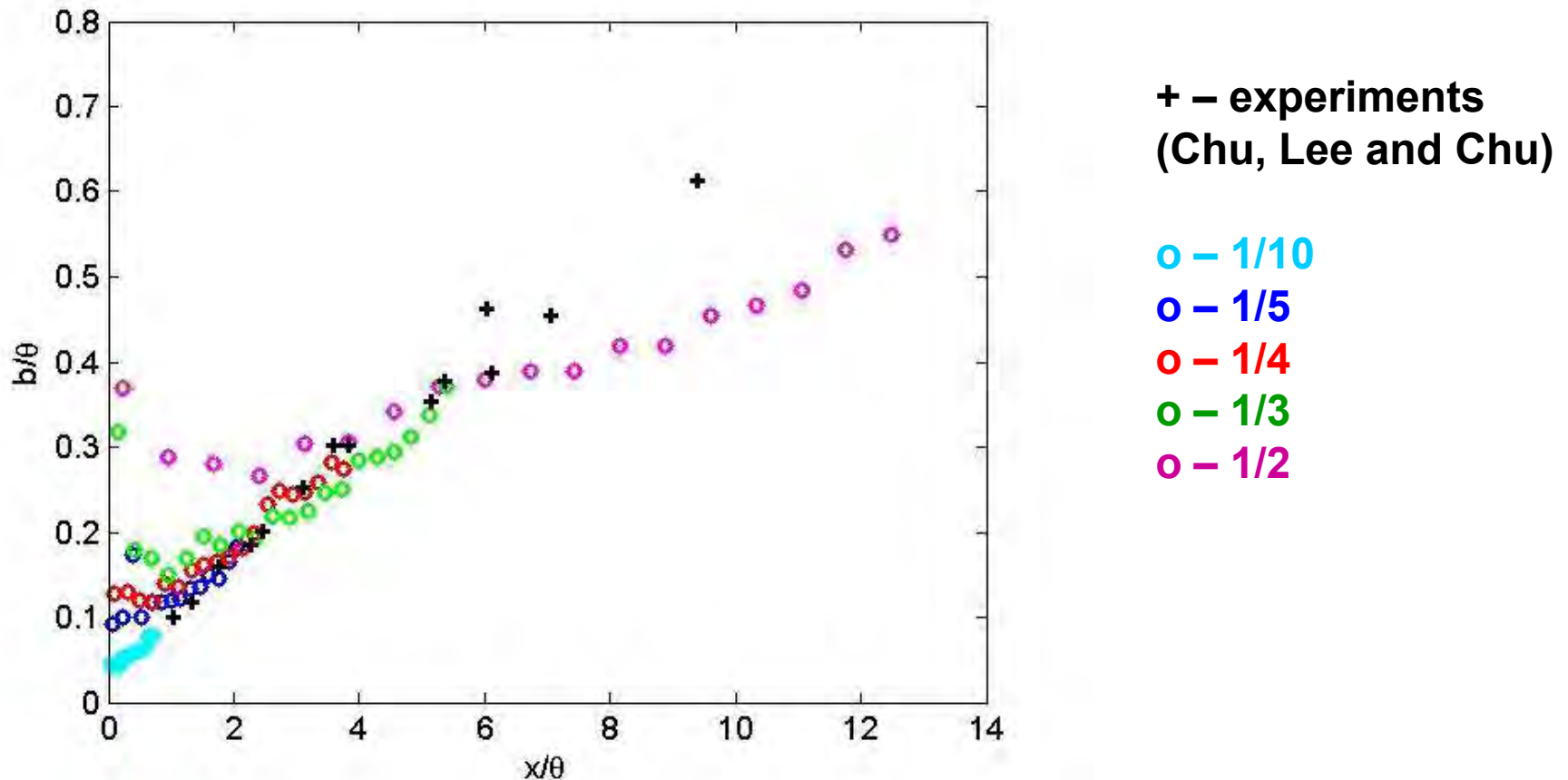
$$U_{\text{excess}} = (U_{\text{centerline}} - U_{\text{coflow}})/U_{\text{coflow}}$$



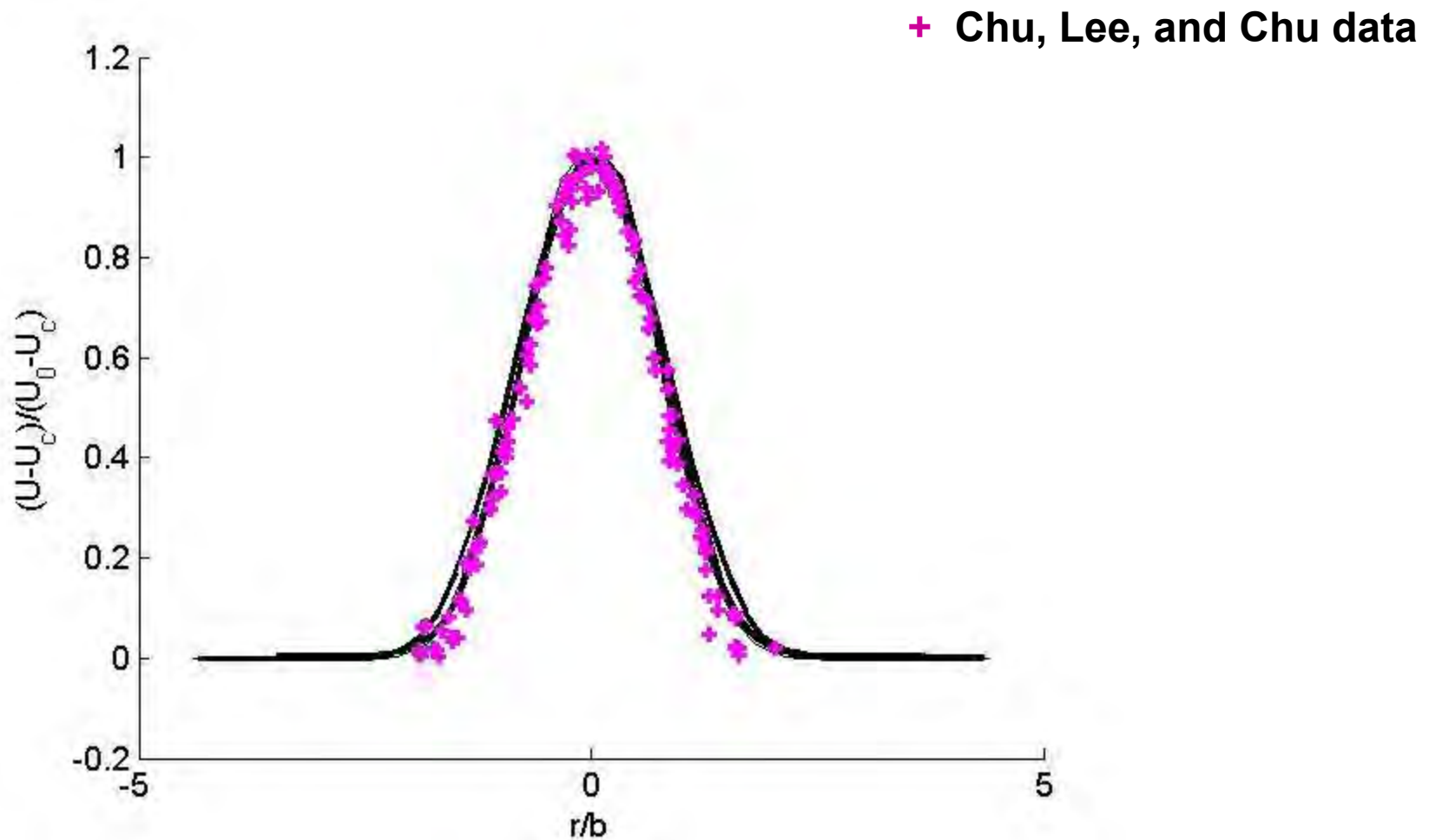
## $\delta/\theta$ vs. streamwise position



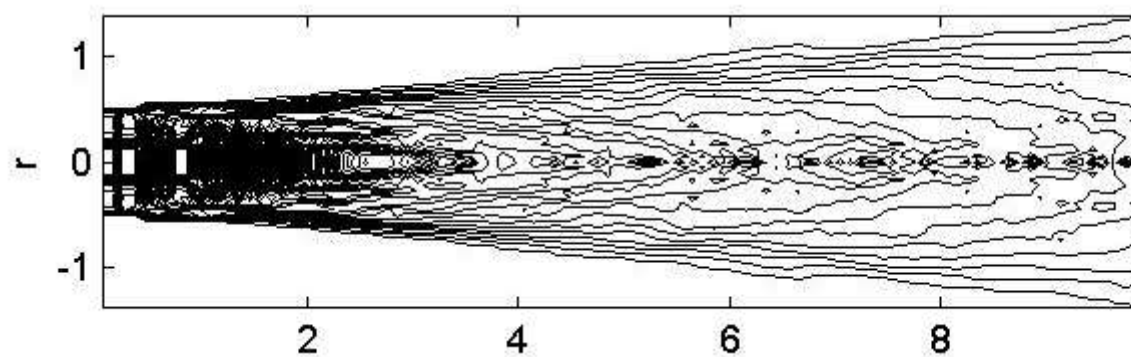
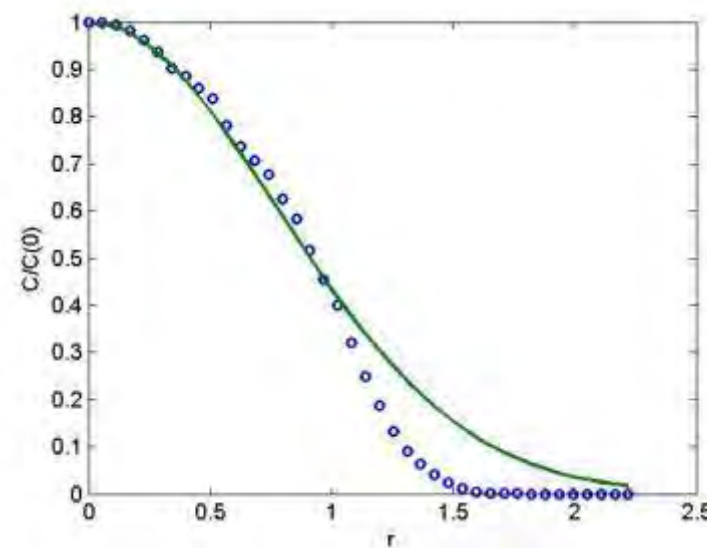
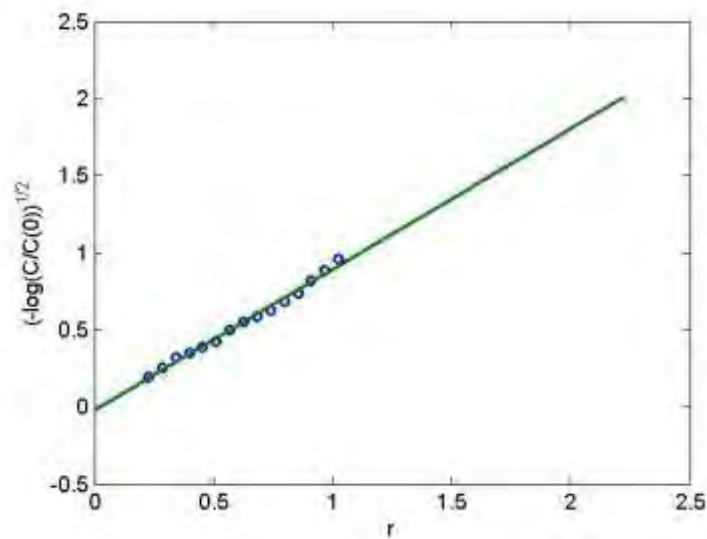
## $b/\theta$ vs. streamwise position



## Self-similar Gaussian mean velocity in coflowing round jet



# Concentration Statistics



**The vortex filament approach appears to offer an attractive means for efficiently simulating a variety of complex turbulent flows.**

**Good resolution of the wall region flow is essential to accurate predictions. Further improvements to the numerical implementation (e.g. parallelism) will enable the treatment of higher Reynolds number flows.**

**The use of vortex filaments in directly representing vortical structure is seen to offer a view of the physics that has not been previously achieved with grid-based methods.**